# Supporting Information for:

# Using Sterics to Promote Reactivity in *fac*-Re(CO)$_3$ Complexes of Some 'Non-Innocent' NNN-Pincer Ligands.

Sarath Wanniarachchi,[a] Brendan J. Liddle,[a] John Toussaint,[a] Sergey V. Lindeman,[a] Brian Bennett[b] James R. Gardinier*[a]

[a]*Department of Chemistry, Marquette University, Milwaukee, WI 53201-1881.*
[b]*Department of Biophysics, Medical College of Wisconsin, Milwaukee, WI, USA 53226.*

**Table of Contents:**

*[A] Structures*

**Figure S-1.** Structure of H($L^{Me}$).

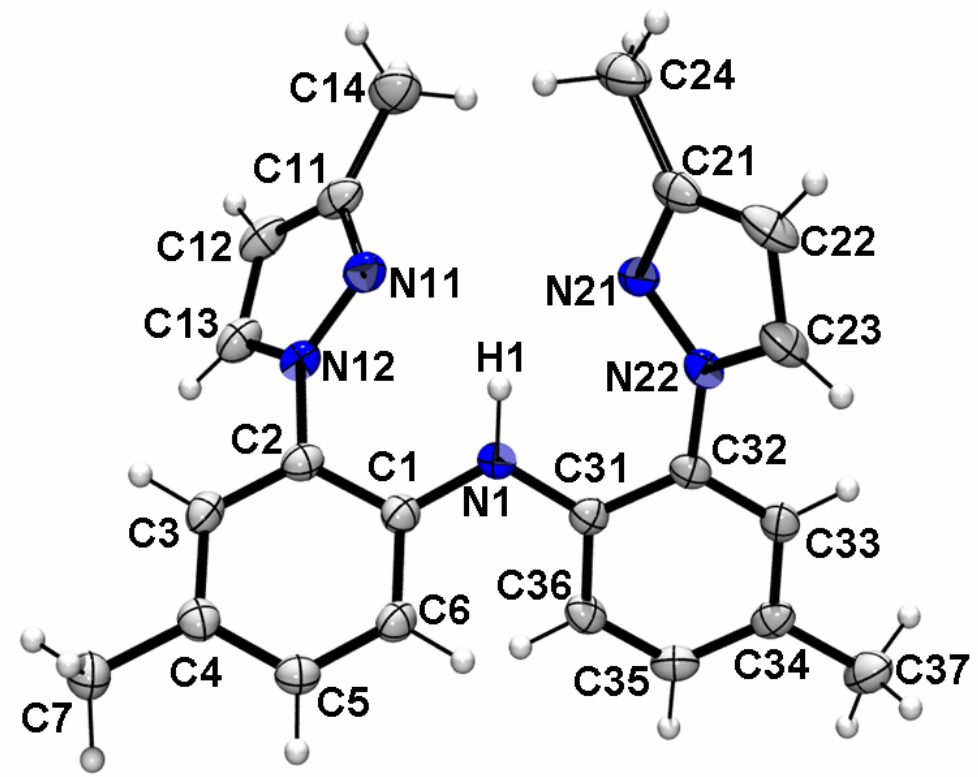

**Figure S-2.** Structure of *fac*-ReBr(CO)$_3$[H(**L**$^{iPr}$)], **1**$^{iPr}$.

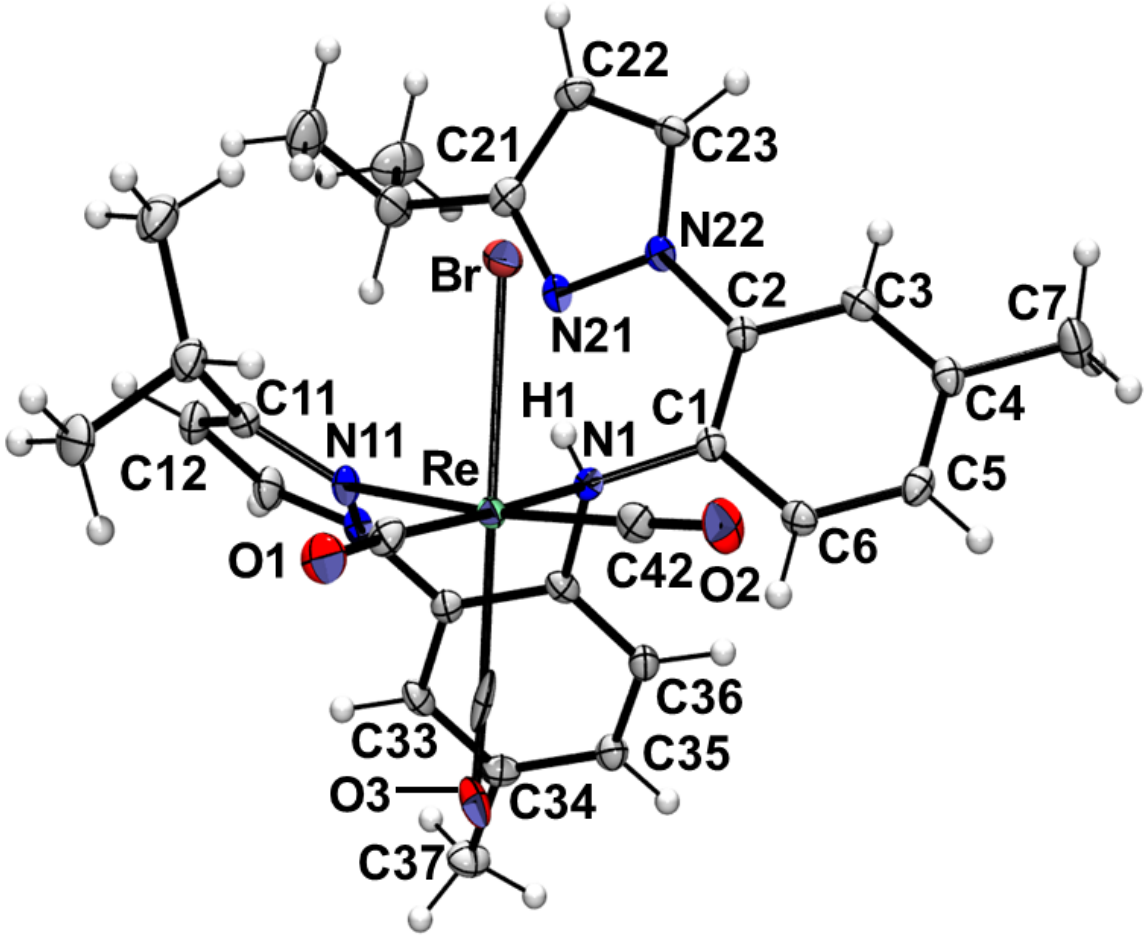

**Figure S-3.** Structure of cation in {*fac*-Re(CO)$_3$[H(**L**$^{iPr}$)]}(PF$_6$), **2**$^{iPr}$. The PF$_6^-$ anion is removed for clarity.

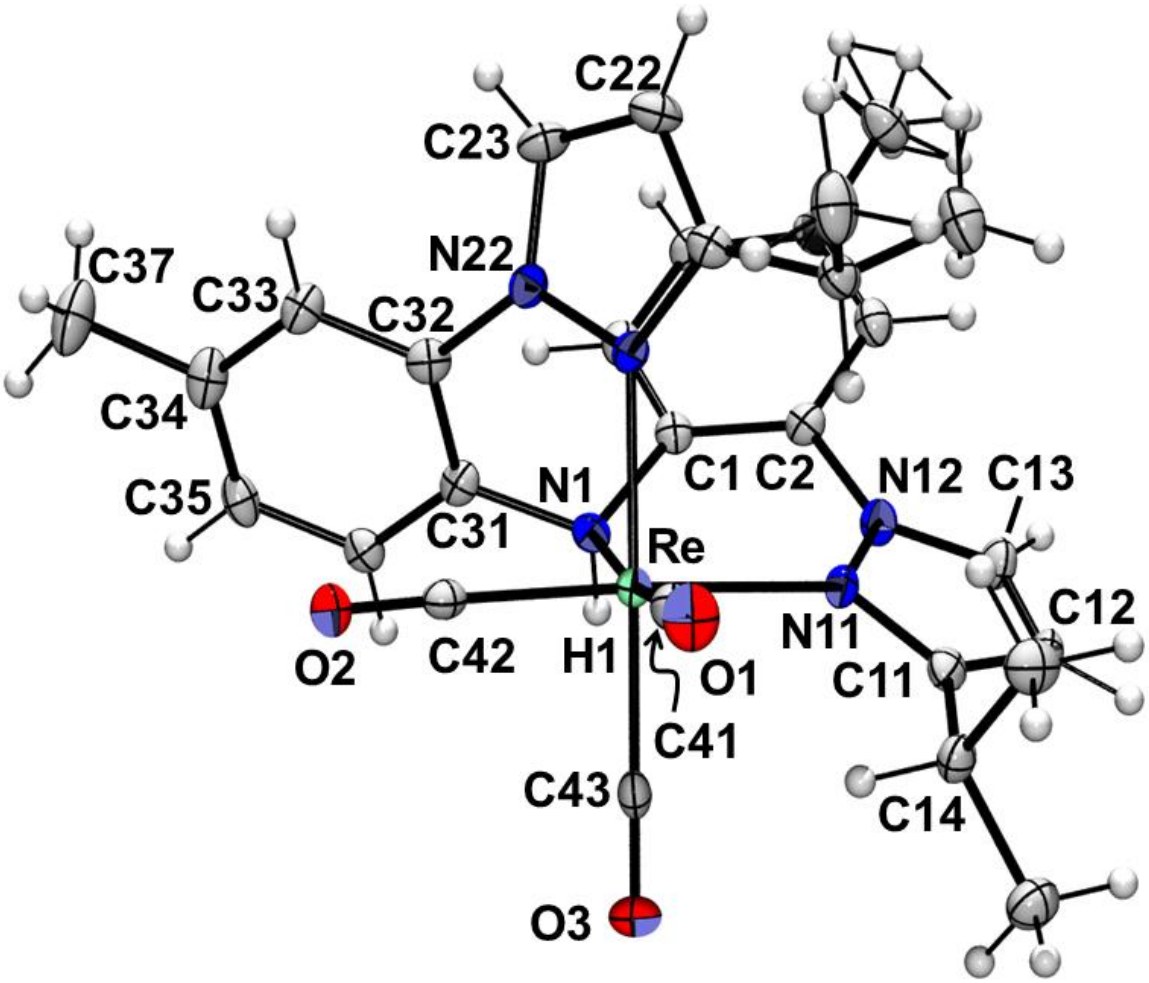

**Figure S-4.** Structure of *fac*-Re(CO)$_3$(**L**$^{iPr}$), **3**$^{iPr}$, with hydrogens removed for clarity.

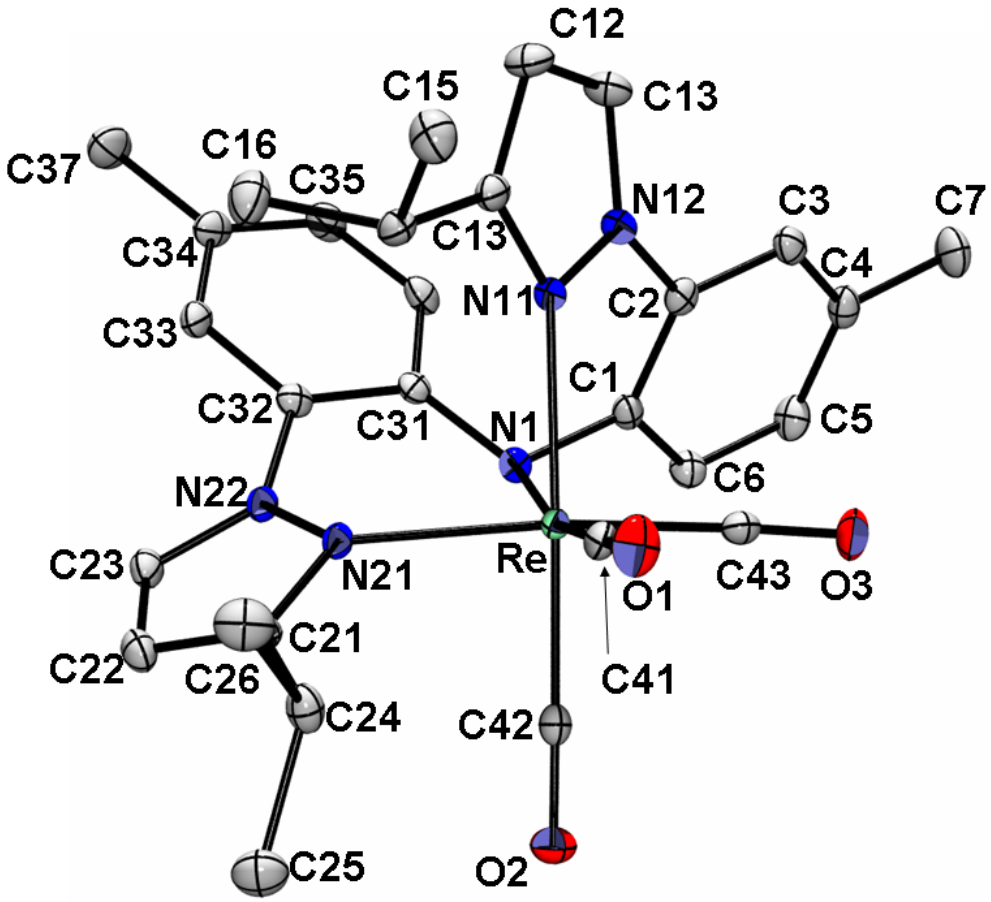

### *[B] NMR spectroscopic Studies*

We previously demonstrated that analytically pure samples of $\mathbf{1^H}$, when dissolved in Lewis donor or chlorocarbon solvents give unexpectedly complex data due to ionization equilibria.[S1] That is, both electrochemical measurements (CV) and solution IR spectroscopy showed multiple signals; one main set of signals was thought to be due to intact $\mathbf{1^H}$ while another set of lower intensity signals was thought to be for $[Re(CO)_3[H(\mathbf{L^H})^+](Br^-)$ based on the similarity of the signals with $\mathbf{2^H}$. As found in Figure S-5, the solid state IR spectrum did not have multiple signals for each C-O stretching mode but the solution spectra does show multiple signals. The ESI(+) MS data of $\mathbf{1^H}$ gave indirect evidence that ionization occurred as the main peak was for the cation, although it is uncertain whether the ionization was due to the

**Figure S-5.** Overlay of IR spectroscopic data for carbonyl stretching region of **1** obtained from (a) KBr pellets and (b) from $CH_2Cl_2$ solutions.

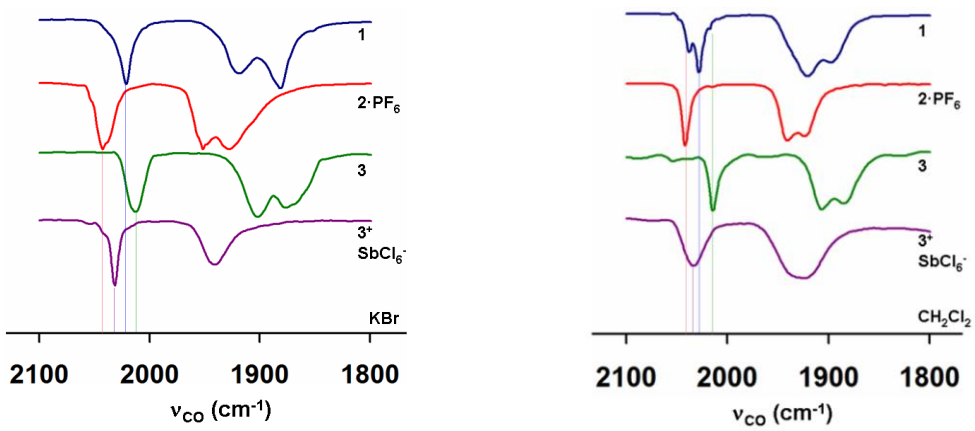


experimental conditions. Furthermore, closer inspection of the NMR data of $\mathbf{1^H}$ in various solvents and that were acquired at various temperatures revealed the existence of a mixture of three species that were tentatively assigned to be: intact $\mathbf{1^H}$ (Fig S-6, right), ionized $[Re(CO)_3[H(\mathbf{L^H})^+](Br^-)$ with a $\kappa^3$N- ligand (Fig S-6, left), and a small amount of a five-coordinate, ionized species with a $\kappa^2$N- ligand where the proton, originally on the central nitrogen of the ligand, is located on a pyrazolyl nitrogen and is hydrogen-bonded to the bromide counter ion (Fig S-6, center). The identity of this latter species arose from MMFF calculations of various structural possibilities for this third species but was never authenticated. This assignment for the third species also represents a potential intermediate along a mechanistic pathway along an ionization trajectory of intact $\mathbf{1^H}$.

**Figure S-6.** Low-energy (MMFF) geometric and coordination isomers of $ReBr(CO)_3$[**H(L)**].

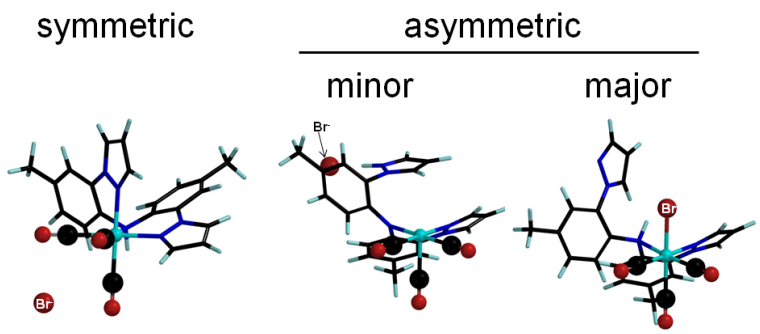


For $\mathbf{1^R}$ (R = Me, iPr), the collective IR, electrochemical, ESI(+) MS, and NMR data indicate that multiple species also exist in solution with intact $\mathbf{1^R}$ being the predominant species at room temperature in either dichloromethane or tetrachloroethane. For $\mathbf{1^R}$ (R = Me, iPr), the large disparity in mixture composition renders $^1$H NMR spectroscopy a more suitable (sensitive) method for illustration of mixture composition than IR or CV data. For instance, a comparison of well-resolved region for the $H_4$-pyrazolyl resonances in the $^1$H NMR spectrum is shown in Figure S-7; full and partial NMR spectra for all species are provided in Figures S-8a and Figs S-11 to S-9. For $\mathbf{1^H}$, resonances for three species (*I*, *II*, and *III*) are easily identified in the bottom of Fig S-7. Again, based on different experimental lines of evidence, species *I* was previously[S1]

**Figure S-7.** Comparison of the $H_4$-pyrazolyl resonance regions in the 295 K $^1$H NMR spectra of $\mathbf{1^R}$ (R = H, bottom; Me, middle; iPr, top).

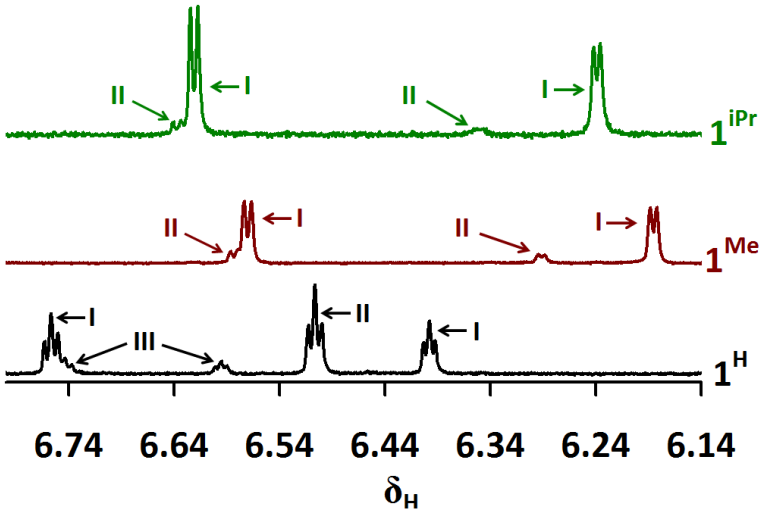


assigned as the intact $\mathbf{1^H}$, species *II* was the six-coordinate ionic species[$Re(CO)_3[k^3N\text{-}H(\mathbf{L^H})^+](Br^-)$], and species *III* was assigned as the five-coordinate ionic species, [$Re(CO)_3[k^2N\text{-}H(\mathbf{L^H})^+](Br^-)$], depicted in the center of Fig S-6. Similarly, for $\mathbf{1^R}$ (R = Me, iPr) confident assignments as to the

two predominant species that exist in halocarbon solutions can be made from the combination of NMR, IR and cyclic voltammetry. For instance, Figure S-8 shows the NMR and IR spectra of the various derivatives **1**$^{Me}$, **2**$^{Me}$, and **3**$^{Me}$ which demonstrate that when **1**$^{Me}$ is dissolved in $CH_2Cl_2$, the major species in the resulting mixture is **1**$^{Me}$ while the minor component is likely $[Re(CO)_3[\kappa^2 N\text{-}H(\mathbf{L}^{Me})^+](Br^-)$ given the similarity of the $^1$H NMR resonances and C-O stretching frequencies between **2**$^{Me}$ and the minor component of the mixture obtained from **1**$^{Me}$. The subtle differences in the signals for **2**$^{Me}$ and $[Re(CO)_3[\kappa^2 N\text{-}H(\mathbf{L}^{Me})^+](Br^-)$ are likely due to the

**Figure S-8**. Comparison of the up-field (methyl) region of the $^1$H NMR spectra and the C-O stretching region of the IR spectrum for **1**$^{Me}$, **2**$^{Me}$, and **3**$^{Me}$ in $CH_2Cl_2$ emphasizing that major component of mixture in $CH_2Cl_2$ is intact **1**$^{Me}$, while the minor component is likely $[Re(CO)_3[\kappa^2 N\text{-}H(\mathbf{L}^{H})^+](Br^-)$.

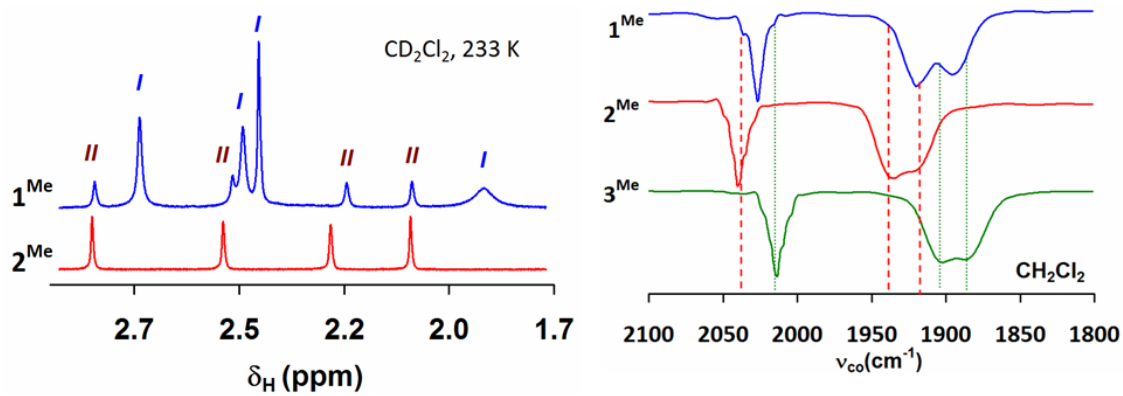


(a) (b)

variable capacity for the different anions to interact (i.e. participate in hydrogen bonding interactions) with acidic protons in the complexes. It is noted from the IR and NMR spectrum of dichloromethane solutions species attributed to ionization isomers of **1**$^{Me}$ are less abundant than those in **1**$^{H}$. In the case of **1**$^{iPr}$, the minor ionization isomers are even less abundant than in **1**$^{Me}$ (Figs. S-9, S-15, and S-16).

**Figure S-9**. Comparison of the C-O stretching region of the IR spectrum of **1**$^{iPr}$, **2** $^{iPr}$, and **3** $^{iPr}$ in $CH_2Cl_2$.

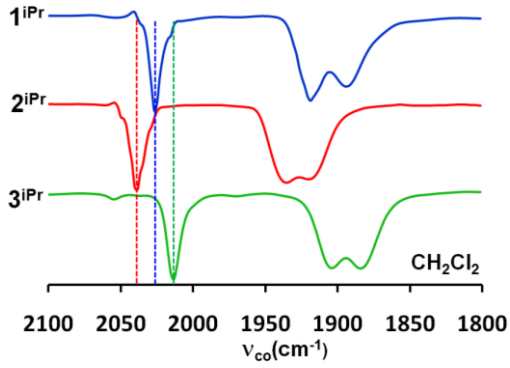

**Fig S-10.** Top: Temperature and solvent-dependent composition of mixtures obtained by dissolving pure **1**$^{Me}$ in $CD_2Cl_2$(left) or $C_2D_2Cl_4$ (right) as measured by relative integration $^1$H NMR resonances in $H_4$-pz region of spectra. Bottom: Similar plots for $CD_2Cl_2$(left) or $C_2D_2Cl_4$ (right) solutions of **1**$^{iPr}$ but very minor resonances for thirds species not shown owing to poor signal-to-noise (see ensuing figures) that hinders reliable integrations.

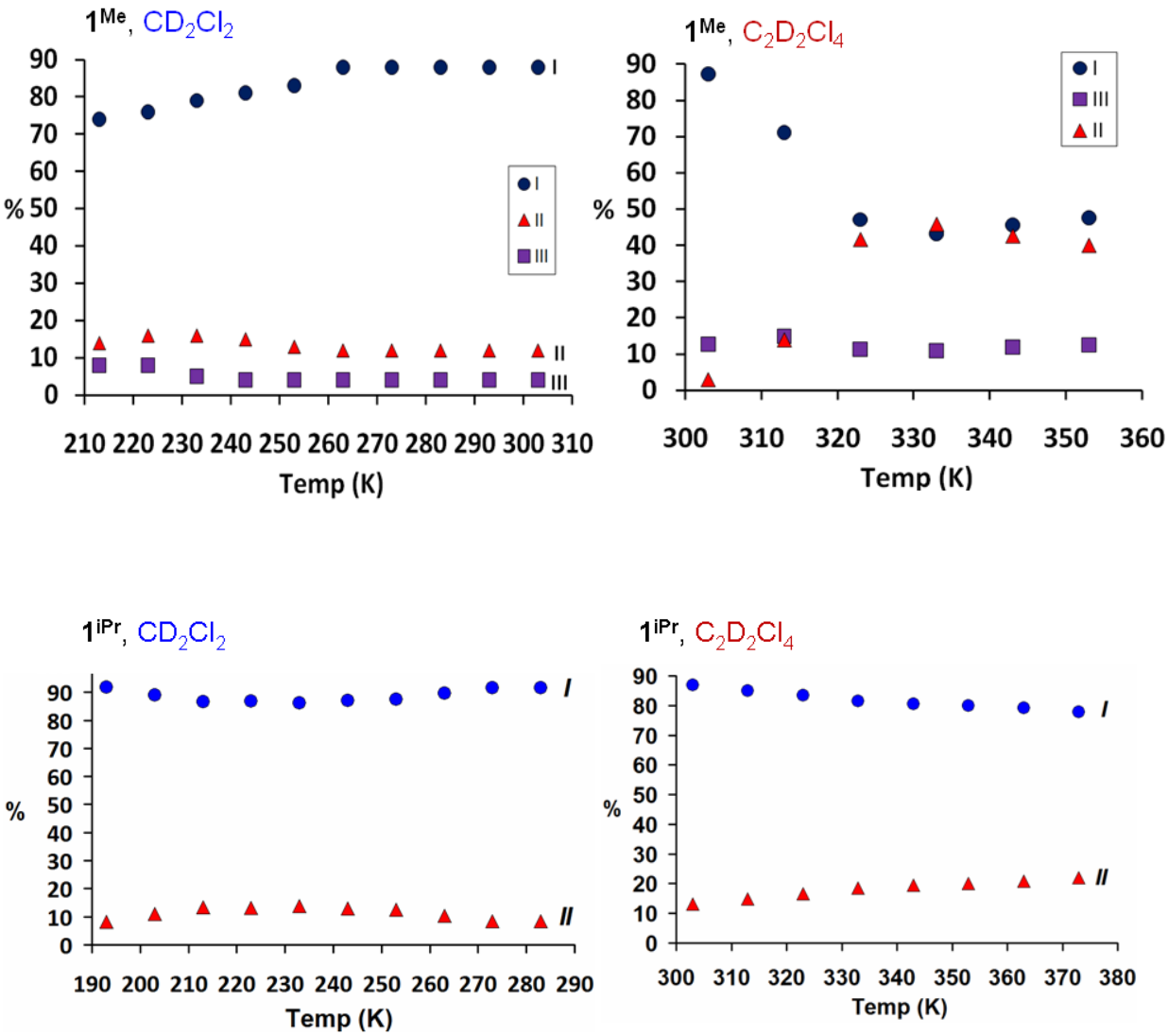

**Figure S-11.** Variable (Low) temperature $^{1}$H NMR spectra of **1**$^{Me}$ in $CD_2Cl_2$ between 193 K and 303 K. (a) aromatic region, (b) methyl region.

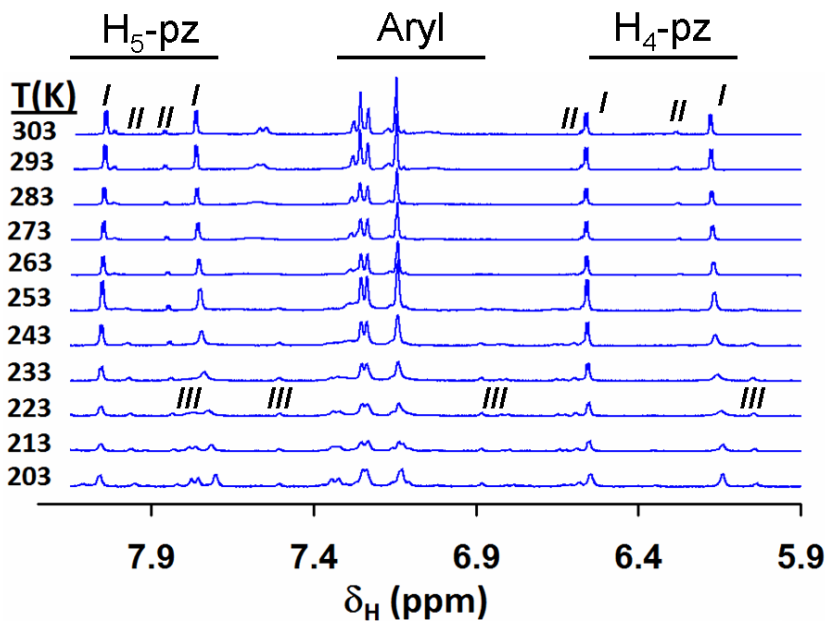


(a)

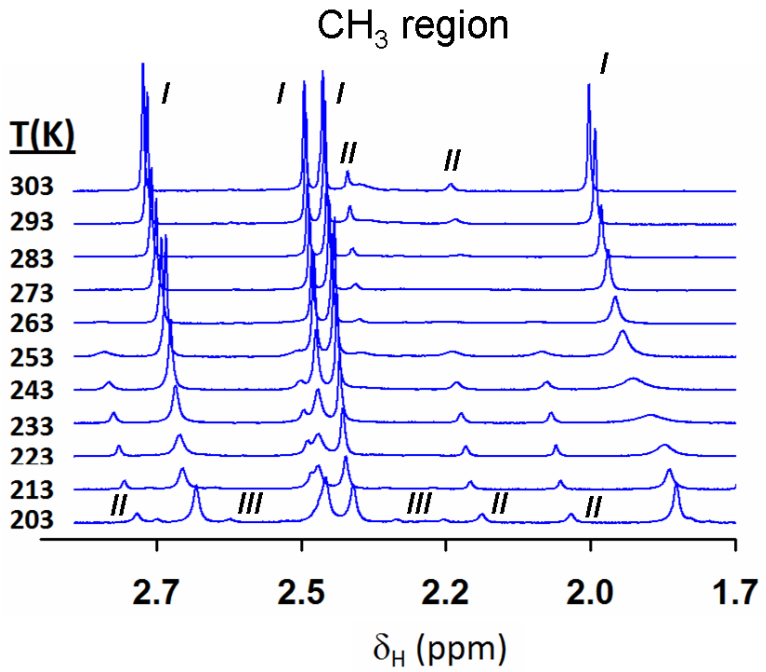


(b)

**Figure S-12.** Variable (High) temperature $^{1}$H NMR spectra of **1**$^{Me}$ in $C_2D_2Cl_4$ between 293 K and 393 K. (a) N-H region, (b) aromatic region.

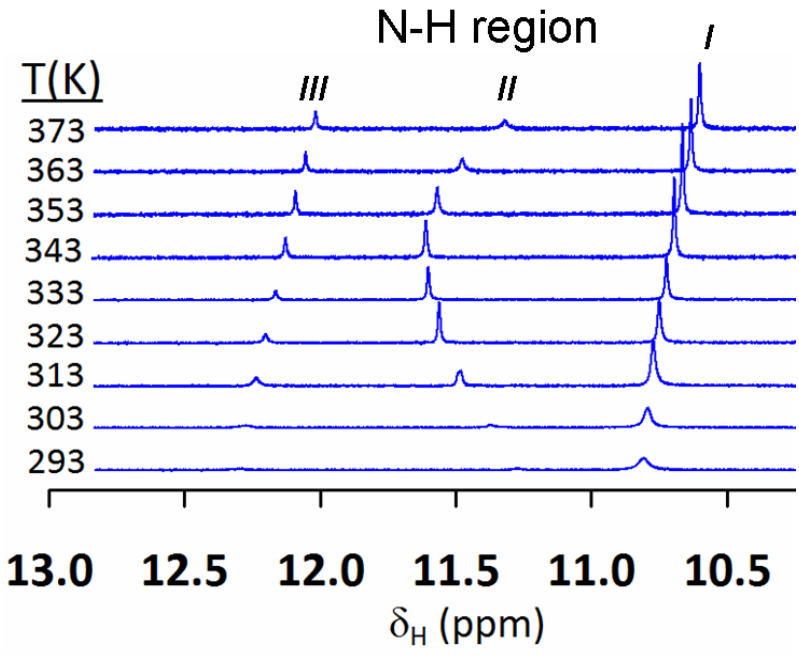


(a)

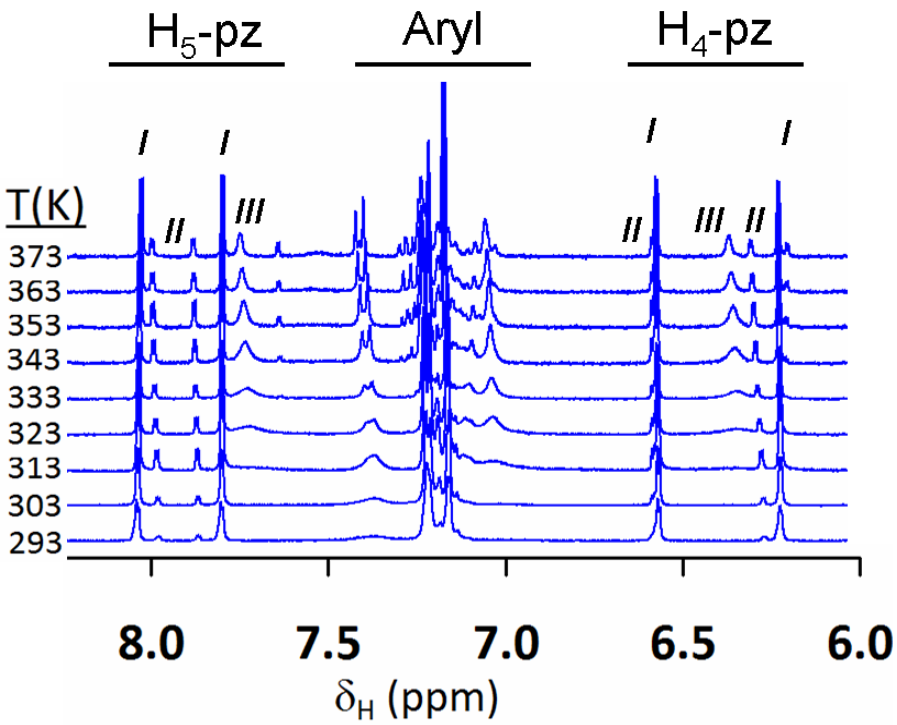


(b)

**Figure S-13.** The NOESY $^{1}H$ NMR spectrum (400 MHz) of **1**$^{Me}$ in $C_2D_2Cl_4$ at 313 K.

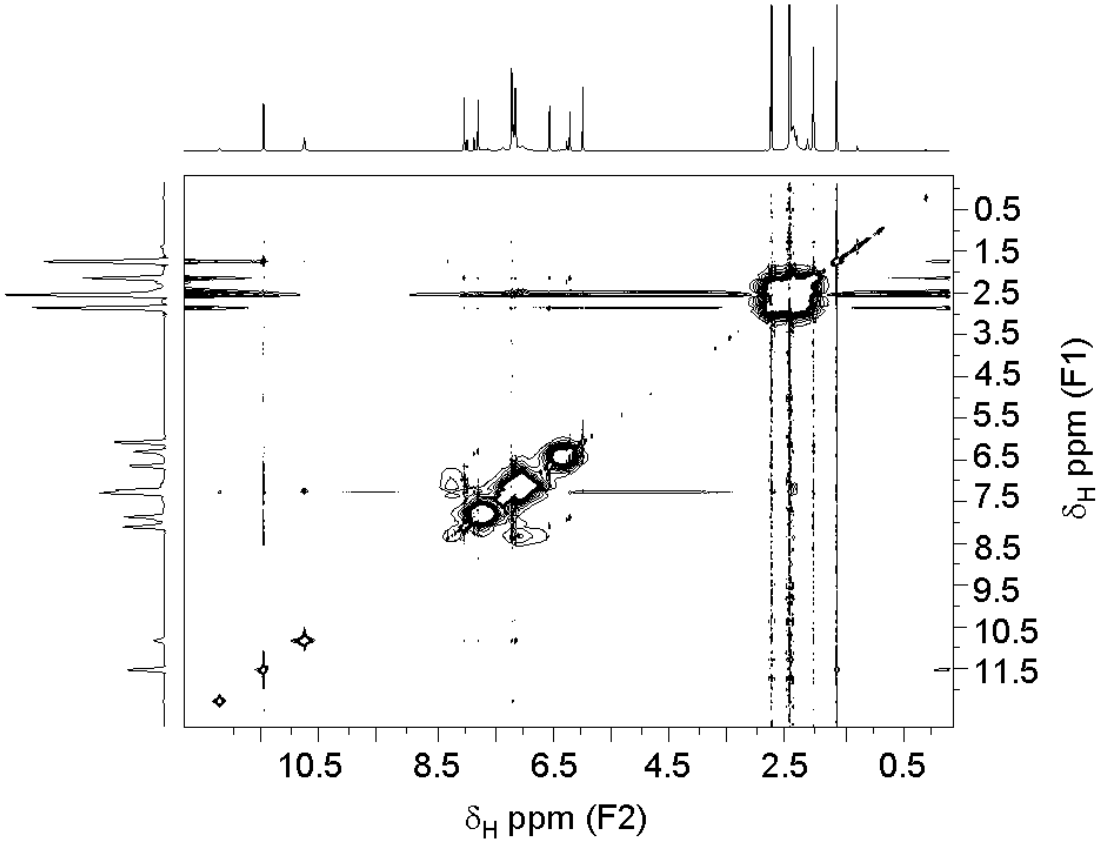

**Figure S-14.** The DQCOSY $^{1}$H NMR spectrum (400 MHz) of **1**$^{iPr}$ in $CD_2Cl_2$ at 293 K.

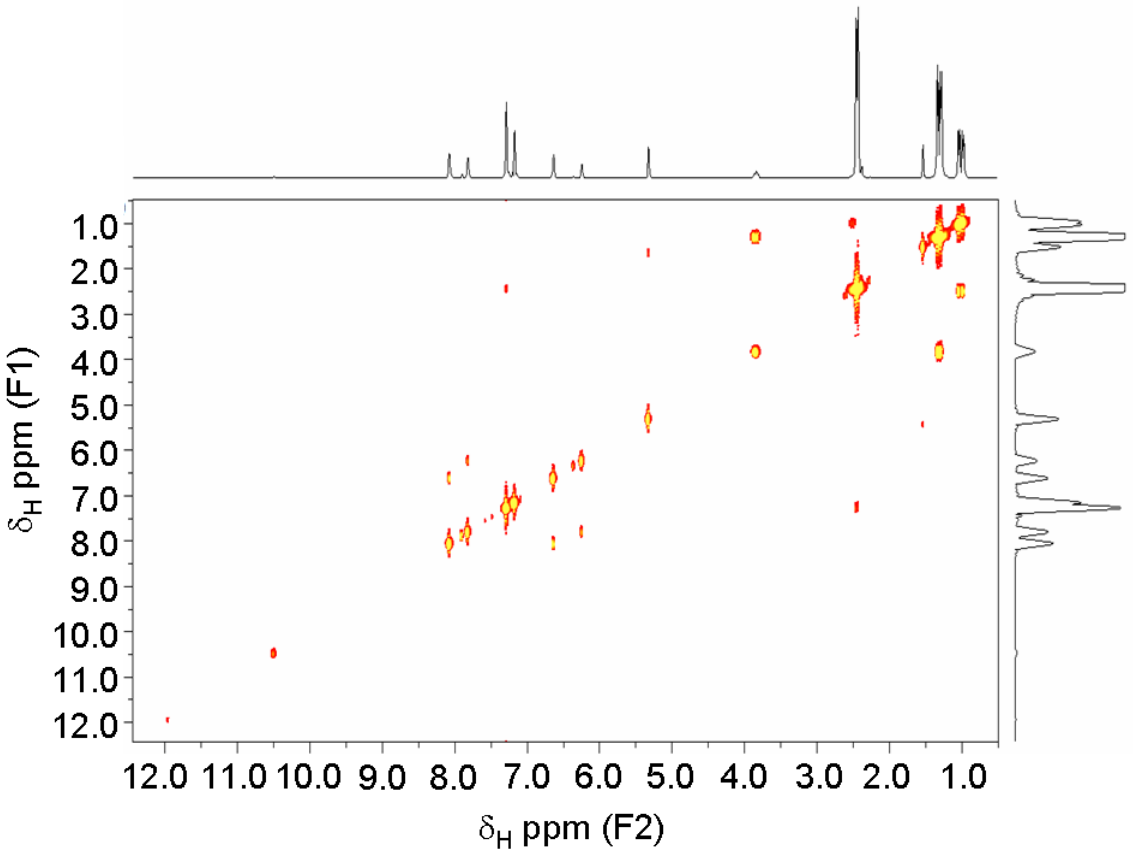

**Figure S-15.** Variable (High) temperature $^1$H NMR spectra of **1**$^{iPr}$ in $C_2D_2Cl_4$ between 293 K and 373 K. (a) Downfield N-H and aromatic regions; (b) upfield region (where $H_2O$ is an impurity in the solvent).

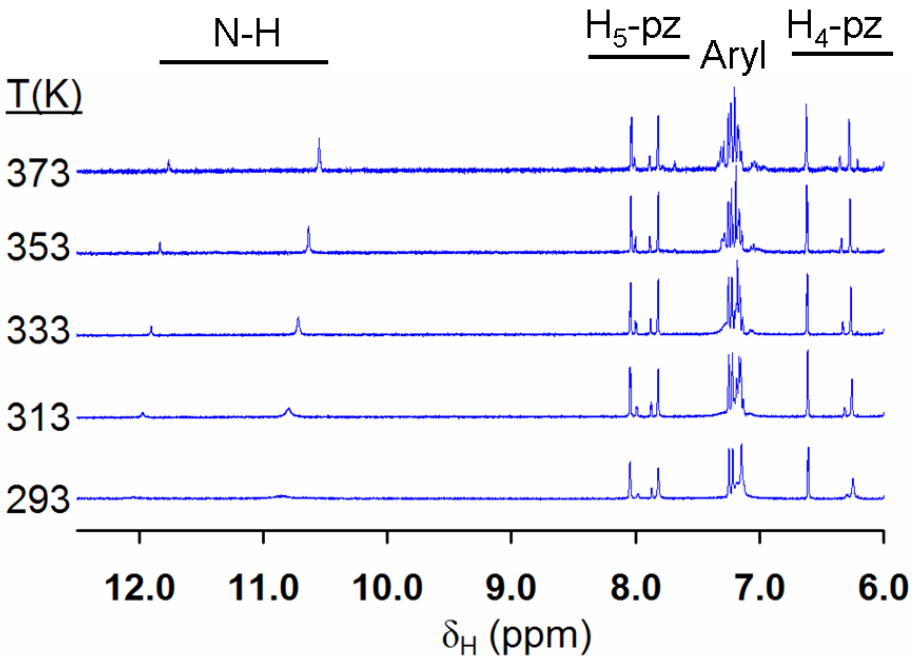


(a)

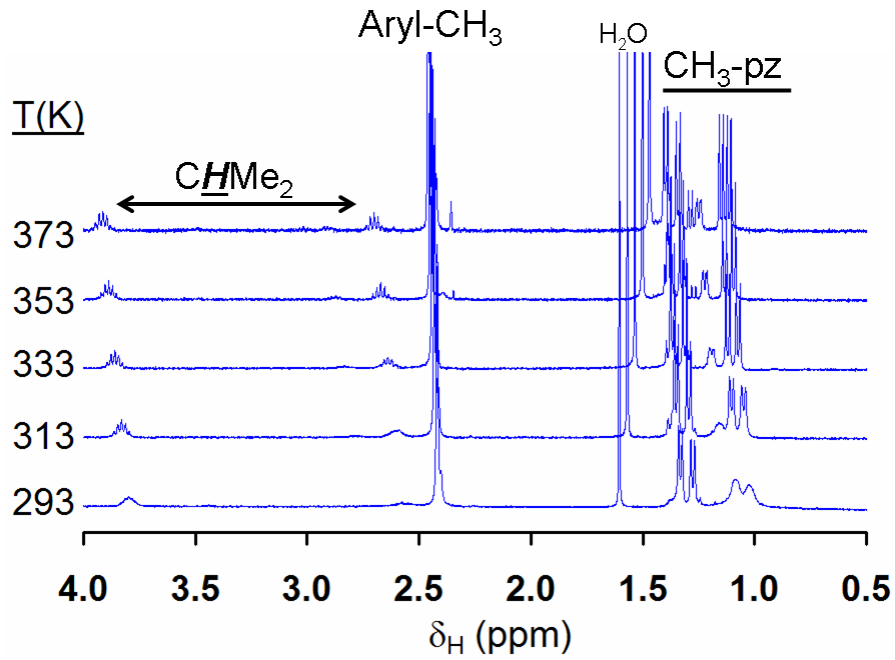


(b)

**Figure S-16.** Variable (Low) temperature $^{1}$H NMR spectra of **1**$^{iPr}$ in $CD_2Cl_2$ between 193 K and 293 K. (a) downfield region, (b) upfield region (where $H_2O$ is an impurity in the solvent).

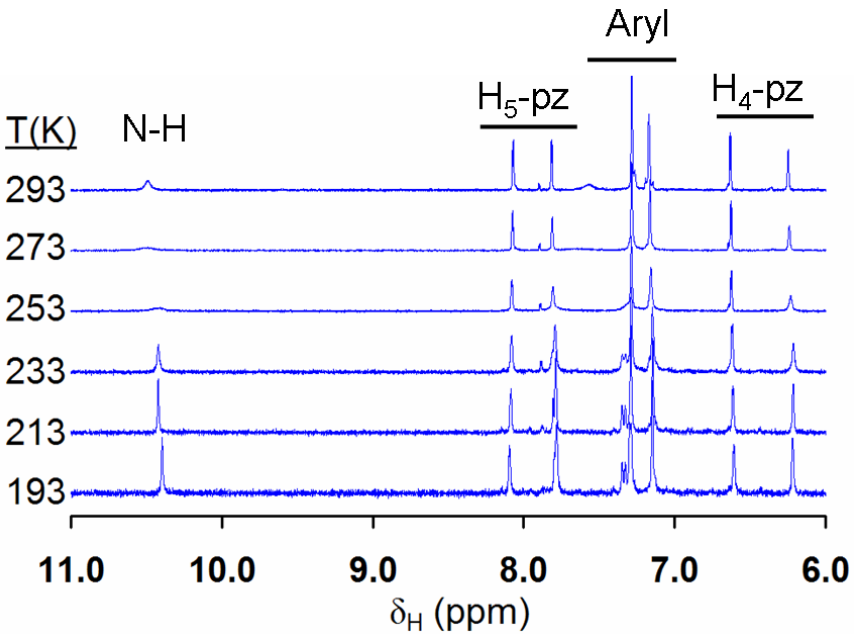


(a)

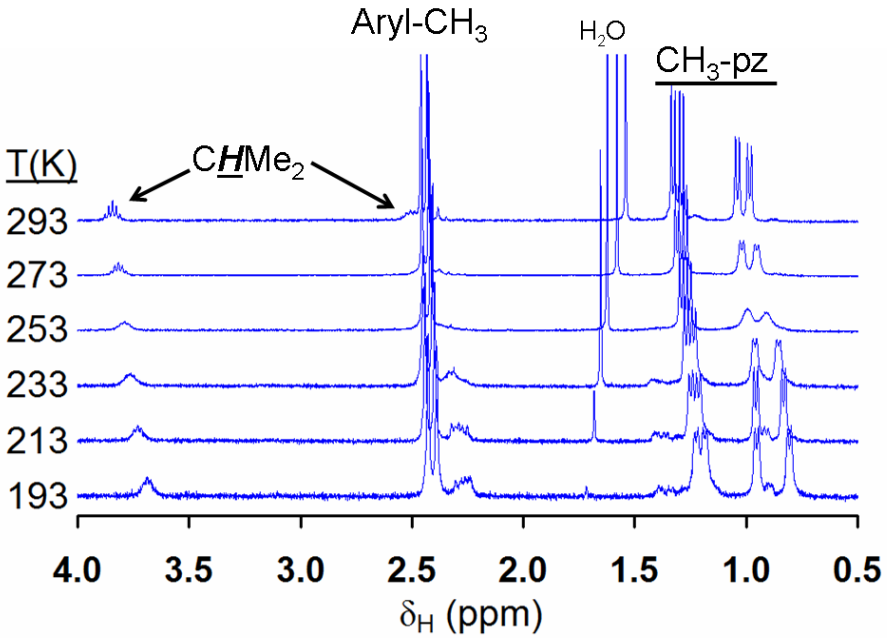


(b)

**Figure S-17.** Variable temperature $^1$H NMR spectra of **2$^{Me}$** in $CD_2Cl_2$ between 193 K and 293 K. (a) downfield region, (b) upfield region.

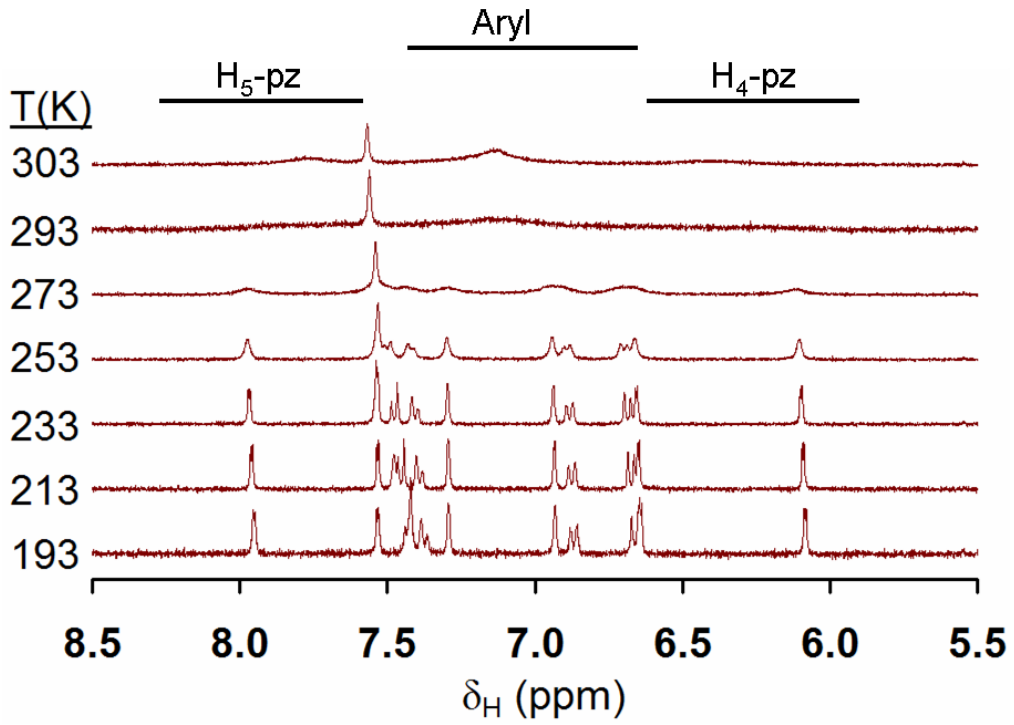


(a)

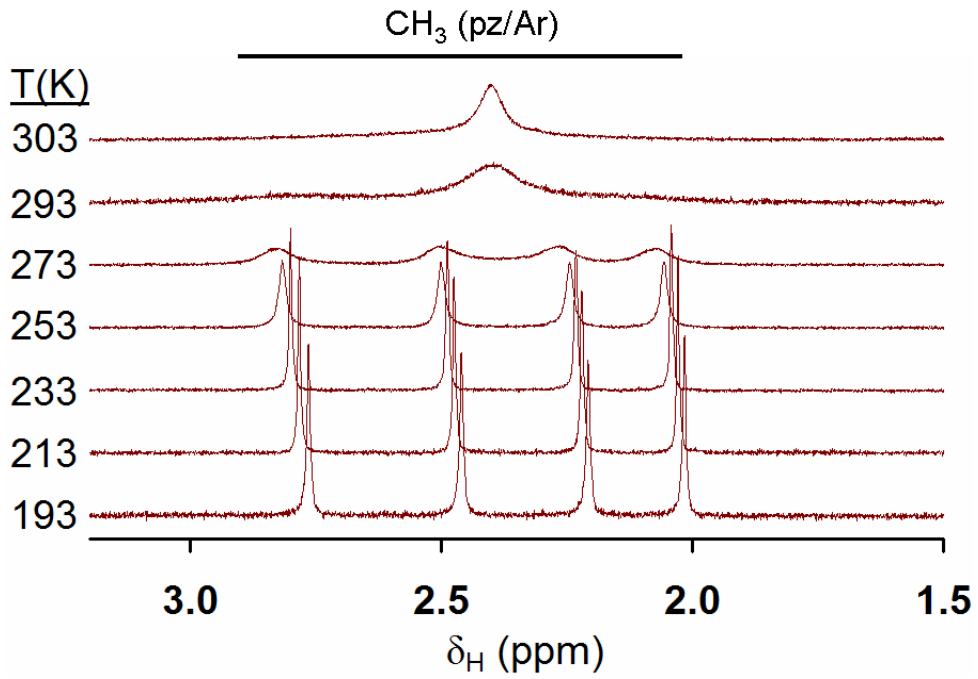


(b)

**Figure S-18.** Variable temperature $^1$H NMR spectra of **2**$^{iPr}$ in $CD_2Cl_2$ between 193 K and 293 K. (a) downfield region, (b) upfield region.

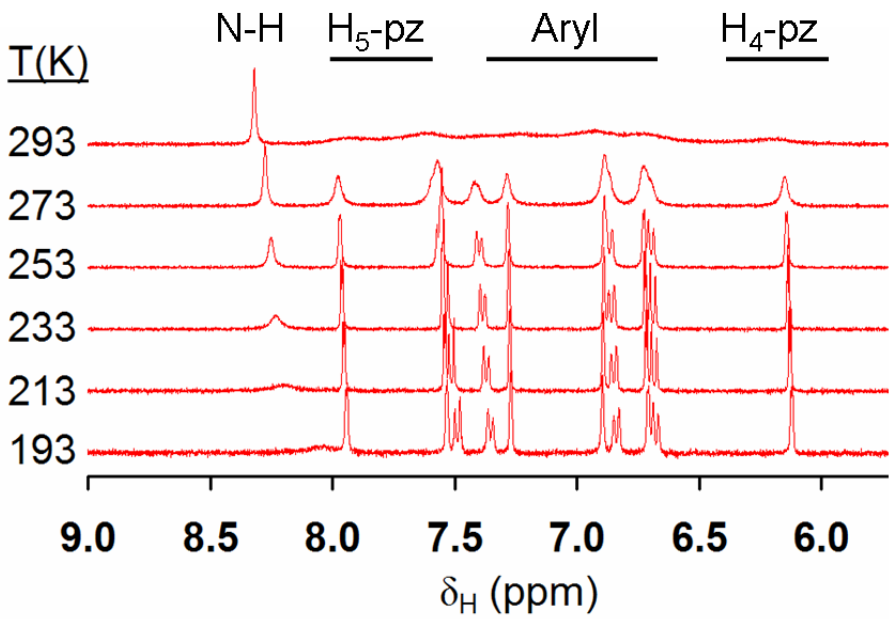


(a)

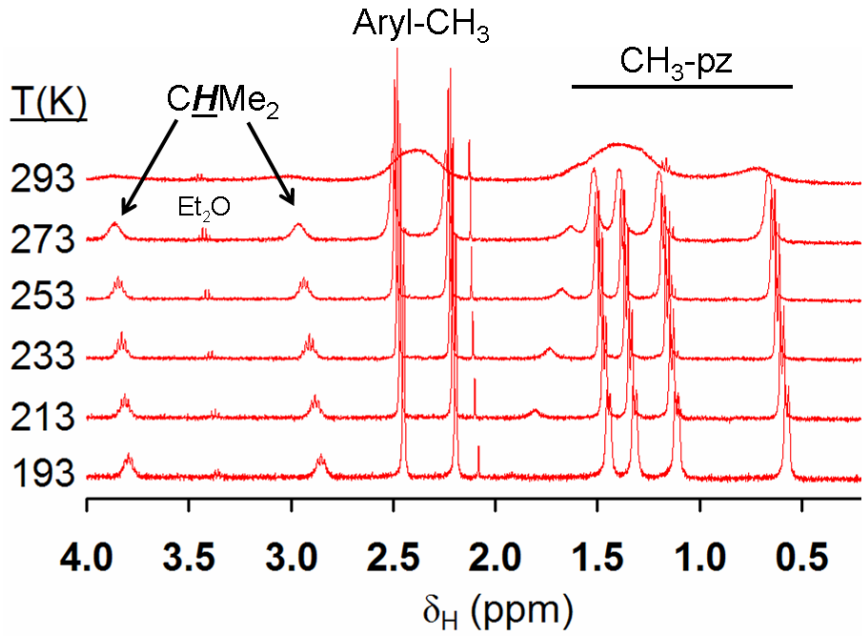


(b)

**Figure S-19.** The $^{1}$H NMR spectra of (a) **3**$^{Me}$ and (b) **3**$^{iPr}$ in $CD_2Cl_2$ between 193 K and 293 K.

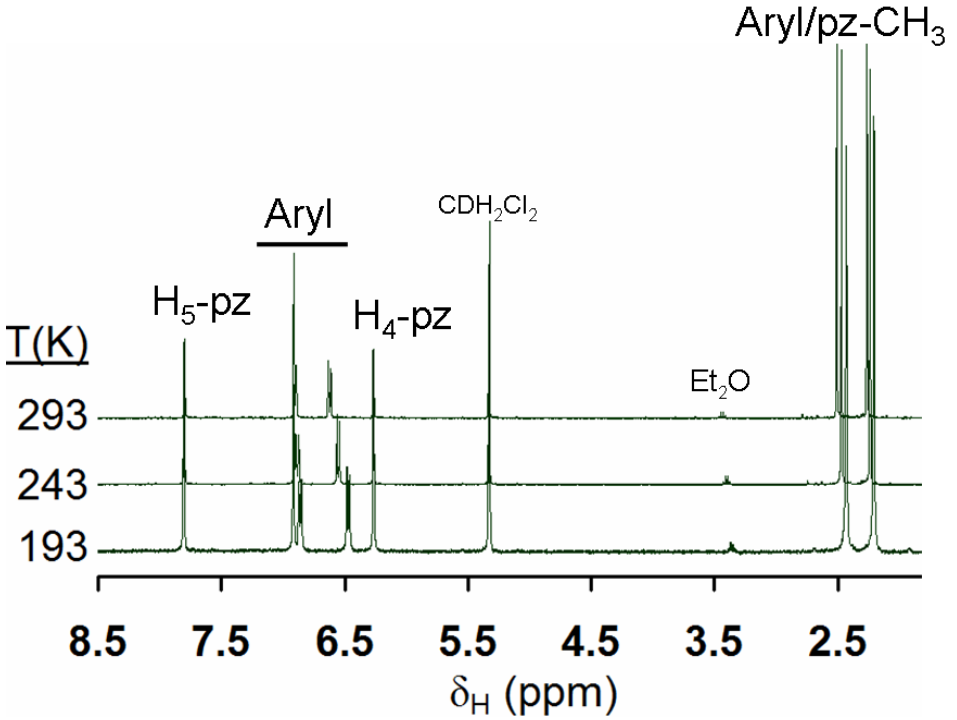


(a)

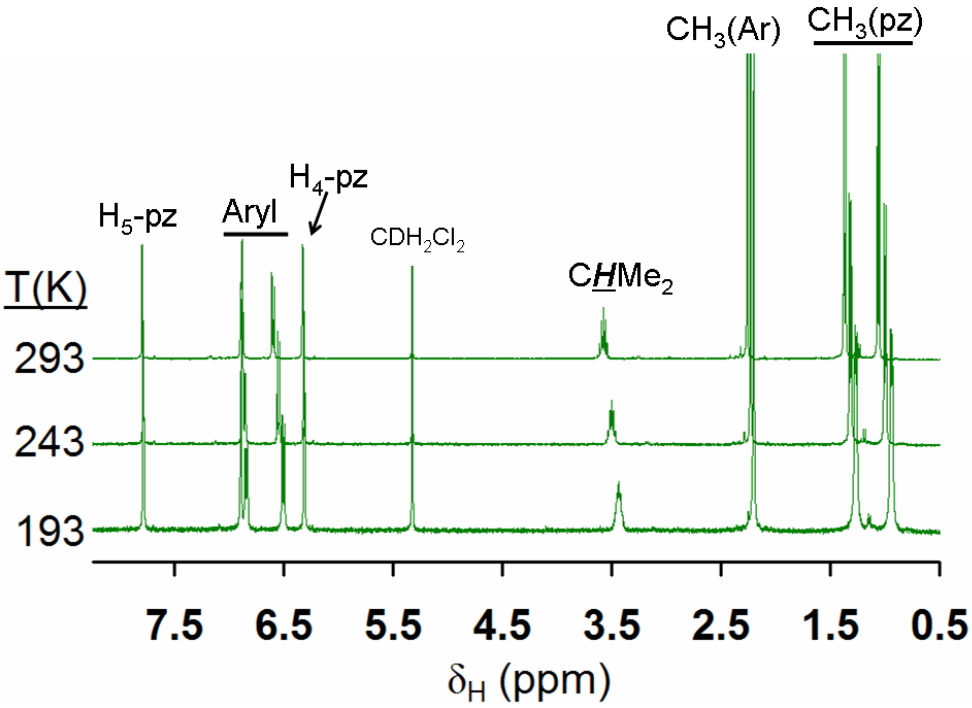


(b)

### *[C] Electrochemistry*

**Fig. S-20.** Cyclic Voltammograms (100 mV/s) of $\mathbf{1}^{R}$ in $CH_2Cl_2$ with $NBu_4PF_6$ as the supporting electrolyte.

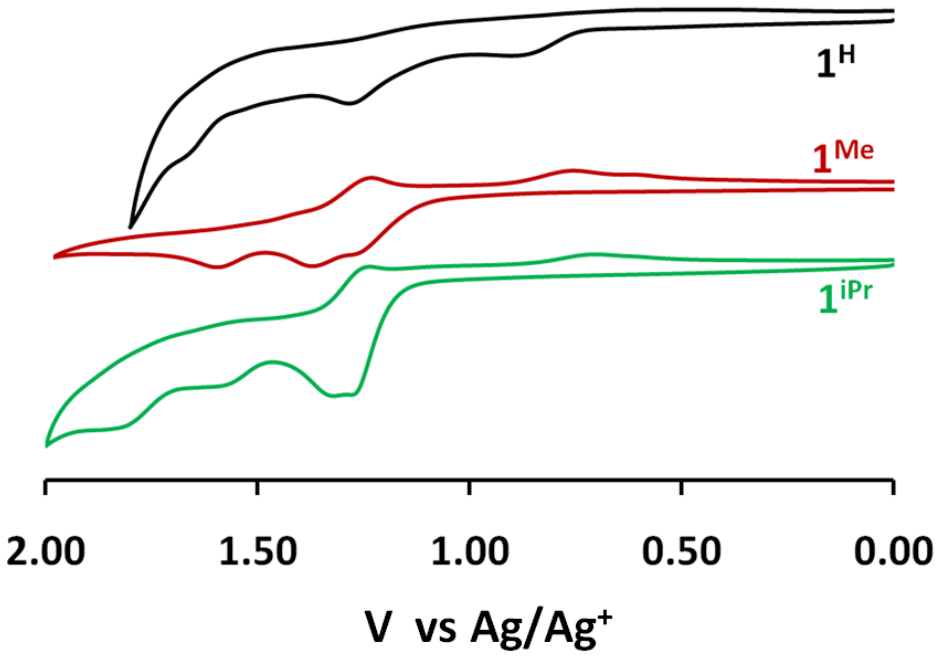


**Fig. S-21.** Cyclic Voltammograms (100 mV/s) of $\mathbf{2}^{R}$ in $CH_2Cl_2$ with $NBu_4PF_6$ as the supporting electrolyte.

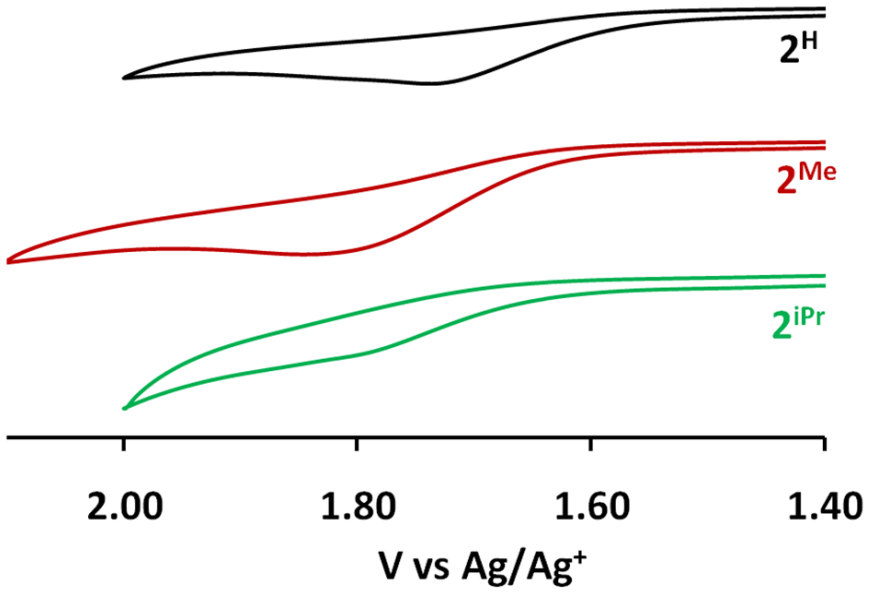

**Fig. S-22.** Scan rate dependence of the cyclic voltammograms of $CH_3CN$ solutions of **3**$^{R}$ (R = Me, iPr) with $NBu_4PF_6$ as the supporting electrolyte.

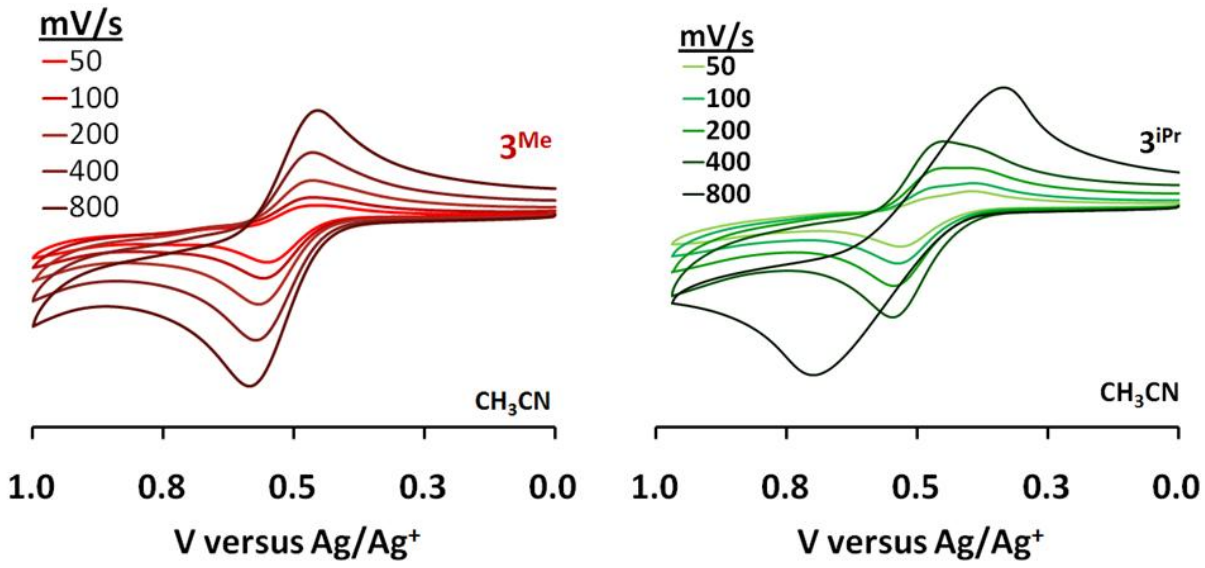

**Fig. S-23.** UV-visible spectra for redox titration between ($CRET^+$)($SbCl_6^-$) and **3**$^{iPr}$ in aerated $CH_2Cl_2$, illustrating the broad pi-radical band near 674 nm. See main narrative for structure of (CRET+).

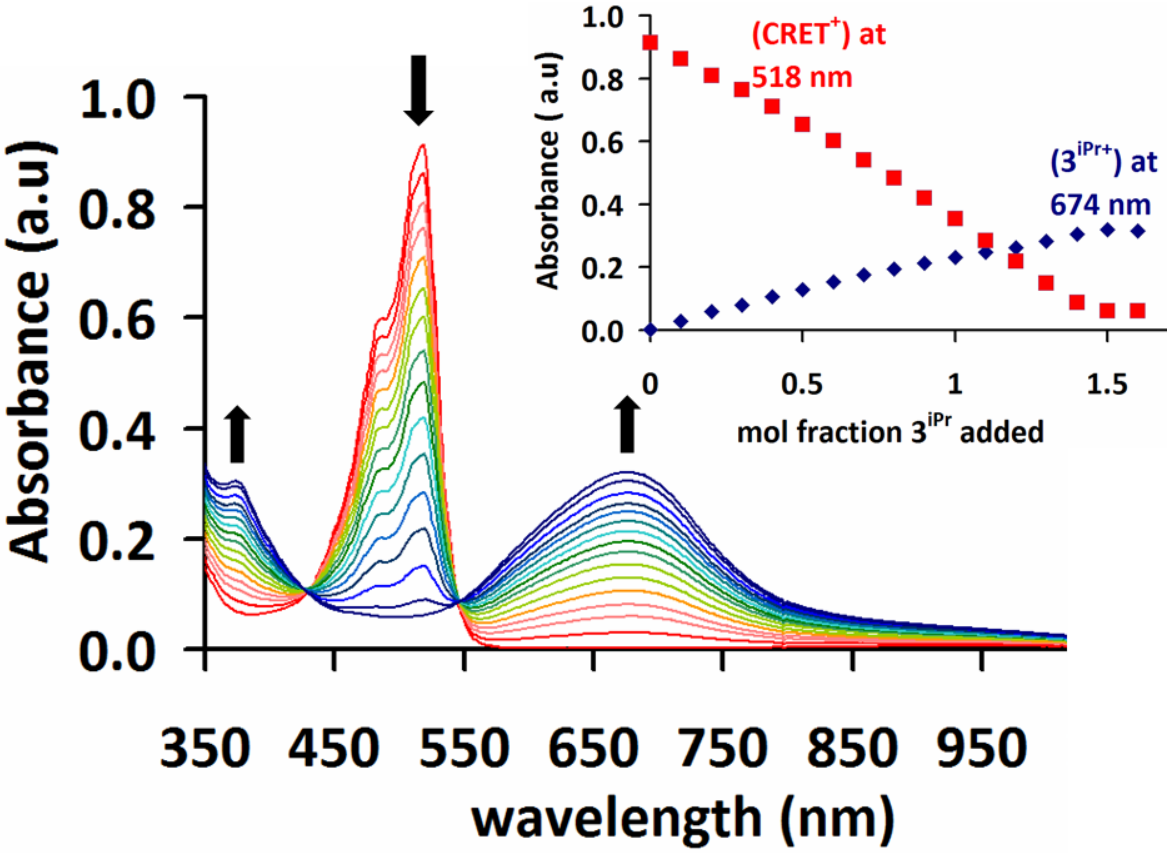

### *[D] Photodecomposition- initial observations.*

Dissolution of either **3**$^{Me}$ or **3**$^{iPr}$ in $CH_2Cl_2$ initially gives a bright yellow solution. Over the course of several hours to several days under ambient lighting conditions (32W, 4100K fluorescent bulbs and glass-filtered sunlight) the solutions turn orange and then red-violet regardless of being contained in either quartz or colorless borosilicate glass containers (Figure S-24). The photodecomposiiton also occurred under exclusion of atmospheric moisture or oxygen. If $CH_2Cl_2$ solutions of **3**$^{Me}$ or **3**$^{iPr}$ are protected from light in foil-covered containers, they remain yellow for weeks even when exposed to air. When red-violet solutions from purposeful photoirradiation of **3**$^{iPr}$ solutions were analyzed by electronic absorption (Figure S-25) and EPR spectroscopy, featureless signals of an unidentified organic cation radical ($\lambda_{max}$ = 475 and 540 nm; $g_{iso}$ = 2.003) were observed. Moreoever, the ESI(+) mass spectrum (Fig. S-26) showed peaks at m/*z* = 720, 743, and 758 consistent with those expected for $ReCl(CO)_3[(M)H(\mathbf{L}^{iPr})]$ (M = H, Na, K from the spectrometer) based on the similar, distinctive fragmentation pattern found for **1**$^{iPr}$. Given the similarity in the electrochemical behavior of **3**$^{R}$, the comparable energy but more intense low energy absorption bands in the electronic absorption spectrum of **3**$^{H}$ versus the other two **3**$^{R}$ compounds (which might be expected to render **3**$^{H}$ rather more susceptible to photochemistry than **3**$^{R}$ based on absorption cross-section), the difference in reactivity of the complexes is likely steric in nature (c.f. accessibility to the central amido nitrogen) rather than being of electronic origin. We are currently continuing investigations into the intriguing photochemistry of **3**$^{R}$.

**Figure S-24.** Photograph of ca. 2 m<u>M</u> $CH_2Cl_2$ solutions of $Re(CO)_3(\mathbf{L^R})$, $\mathbf{3^R}$, that were exposed to ambient lighting for various lengths of time in borosilicate volumetric flasks. All solutions were initially yellow; only the un-substituted $\mathbf{3^H}$ resists photodecomposition.

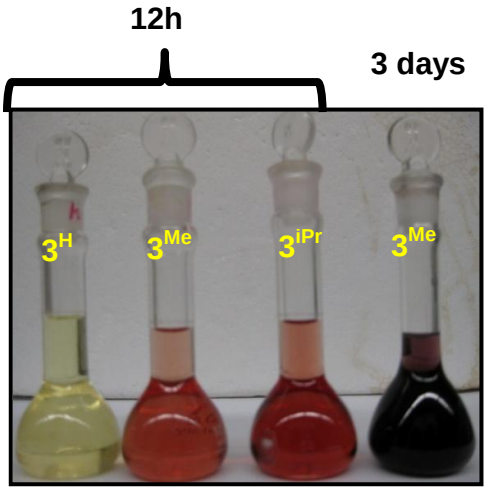


**Figure S-25.** UV-Visible spectra acquired at various time intervals over the period of ten days for aliquots of a 2 m<u>M</u> $CH_2Cl_2$ solution of $\mathbf{3^{Me}}$ (left) and $\mathbf{3^{iPr}}$ (right) contained in the above volumetric flasks and that were exposed to ambient lighting.

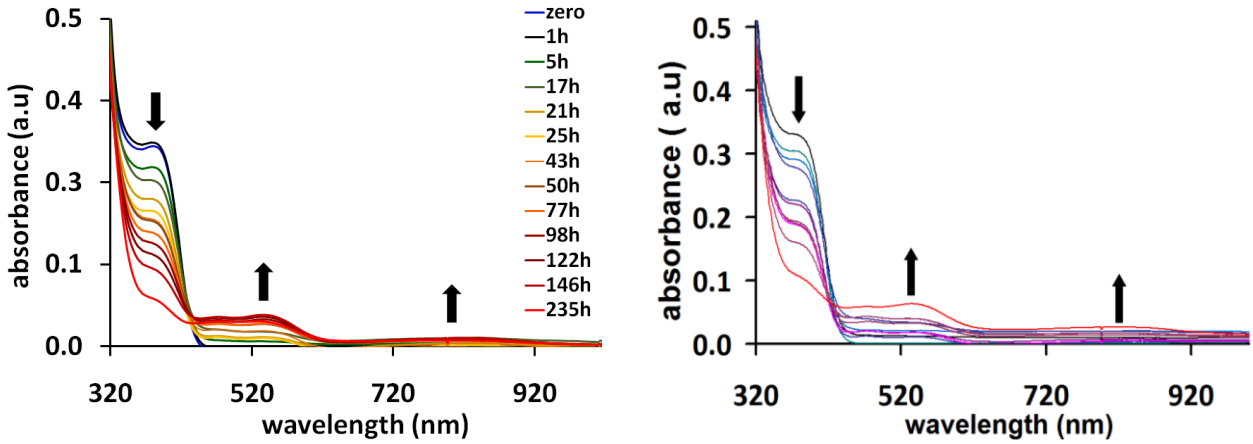

**Figure S-26**. ESI(+) mass spectrum of $CH_2Cl_2$ solution of photodecomposed **3**$^{iPr}$. Structures shown for the assignments are based on empirical formulae and are speculative, as most have not been structurally verified in cases other than m/z = 684.

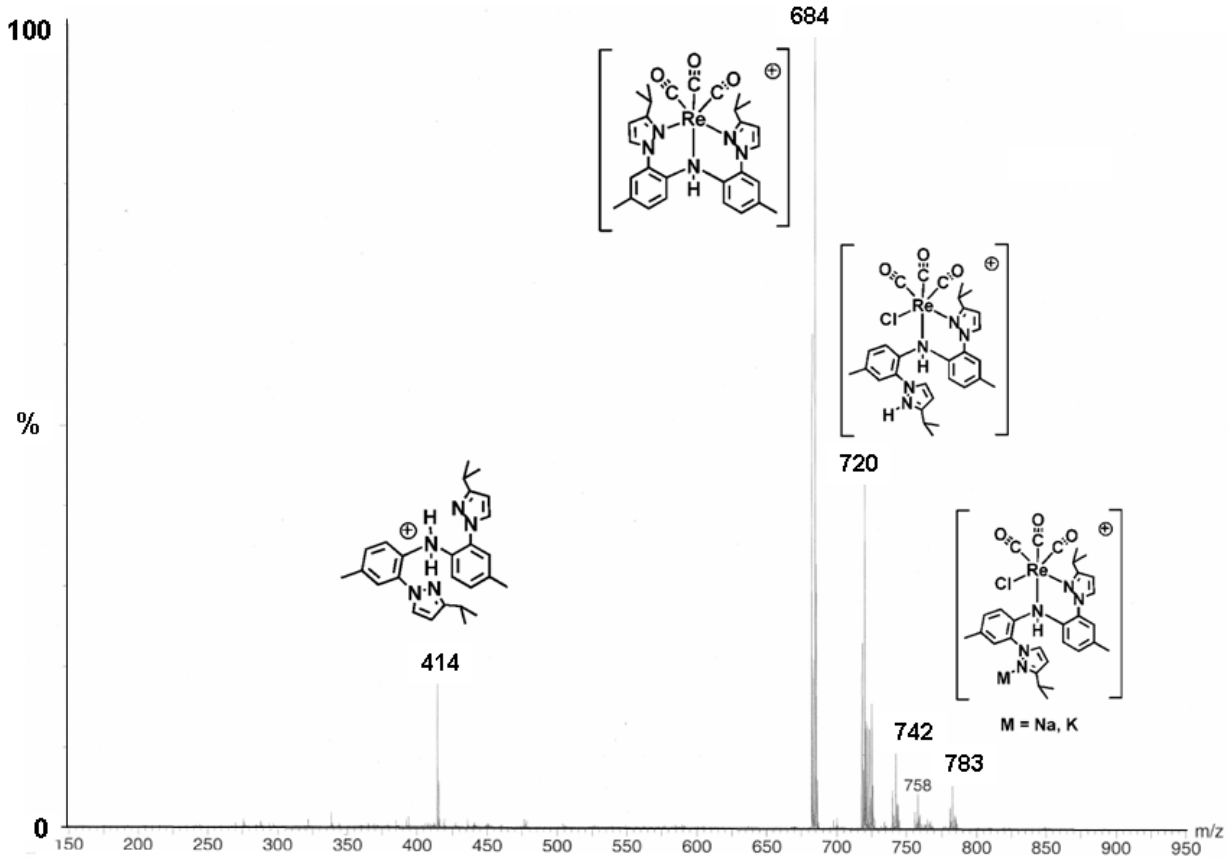

### *[E] Computational Studies*

**General Methods.** Calculations utilized the SPARTAN'06 program suite,[S2] where gas phase structures of the metal complexes (**3**$^{R}$) and (**3**$^{Me+}$) were optimized using the initial geometry from X-ray structural studies of the un-oxidized **3**$^{R}$ as a starting point, then the (u)BP86/6-31G* density functional theoretical model was employed owing to the demonstrated success of this model when applied to other complexes.[S3] Single point energy and time-dependent density functional calculations were performed on the energy-minimized structures using the hybrid B3LYP method, which incorporates Becke's three-parameter exchange functional (B3)[S4] with the Lee, Yang, and Parr (LYP)[S5] correlation functional where the LACVP* effective core potential[S6] basis set was employed for each.

**Fig. S-27.** Frontier Orbitals for *fac*-Re(CO)$_3$(**L**$^{\mathbf{Me}}$), **3**$^{\mathbf{Me}}$ from DFT calculations (B3LYP/LACVP*).

| | | |
|---|---|---|
| 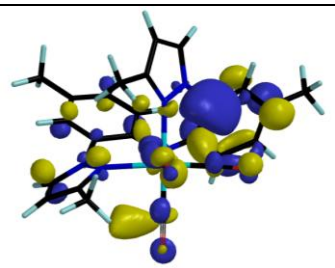 | 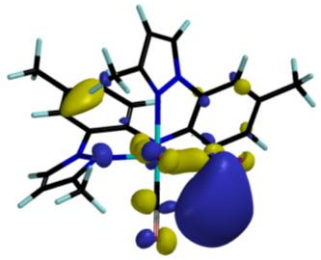 | 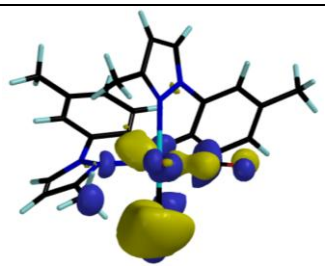 |
| **+3.56 eV** | **+3.78 eV** | **+4.03 eV** |
| **LUMO(+3)** | **LUMO(+4)** | **LUMO(+5)** |

| | | |
|---|---|---|
| 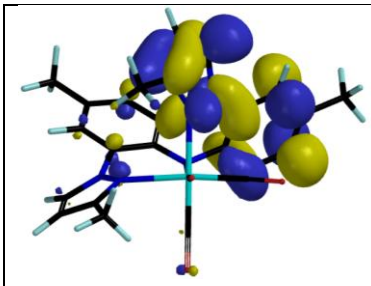 | 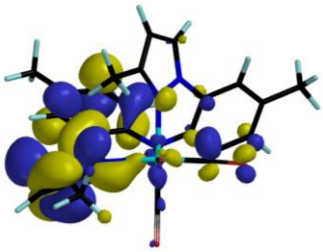 | 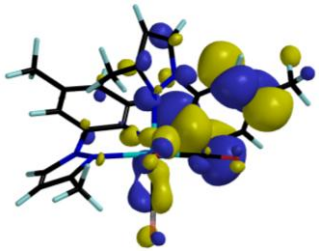 |
| **+2.55** | **+2.99 eV** | **+3.26 eV** |
| **LUMO** | **LUMO(+1)** | **LUMO(+2)** |

| | | |
|---|---|---|
| 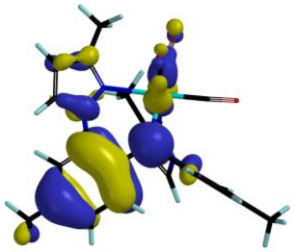 | 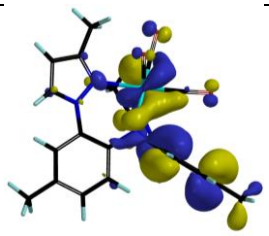 | 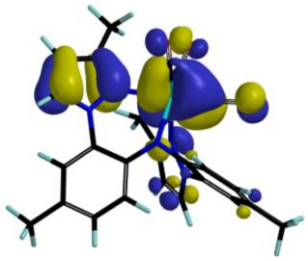 |
| **-6.36 eV** | **-7.75 eV** | **-8.02 eV** |
| **HOMO** | **HOMO(-1)** | **HOMO(-2)** |

**Fig. S-28.** Frontier orbitals of *fac*-Re(CO)$_3$(**L**$^{iPr}$), **3**$^{iPr}$ from DFT calculations (B3LYP/LACVP*).

| | | |
|---|---|---|
| 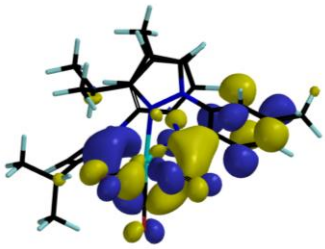 | 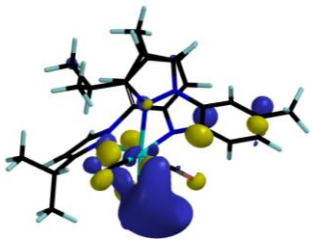 | 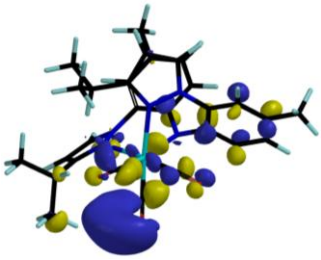 |
| **+3.48 eV** | **+3.66 eV** | **+3.91 eV** |
| **LUMO(+3)** | **LUMO(+4)** | **LUMO(+5)** |

| | | |
|---|---|---|
| 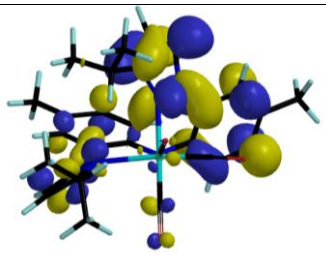 | 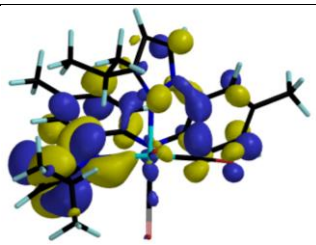 | 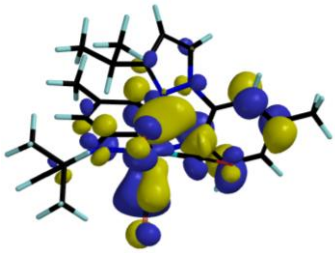 |
| **+2.66** | **+2.91 eV** | **+3.29 eV** |
| **LUMO** | **LUMO(+1)** | **LUMO(+2)** |

| | | |
|---|---|---|
| 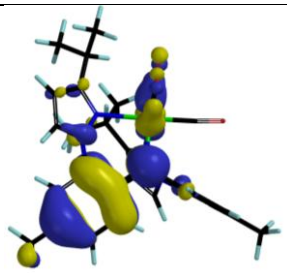 | 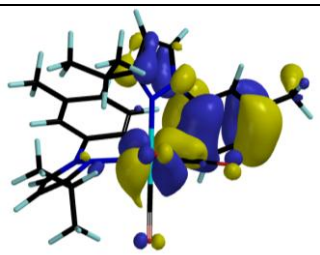 | 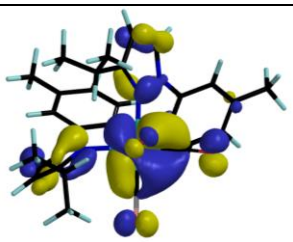 |
| **-6.68 eV** | **-7.94 eV** | **-8.21 eV** |
| **HOMO** | **HOMO(-1)** | **HOMO(-2)** |

**Fig. S-29.** Alpha-Frontier Orbitals for [*fac*-Re(CO)$_3$(**L**$^{Me}$)$^+$], (**3**$^{Me+}$) from DFT calculations (uB3LYP/LACVP*).

| | | |
|---|---|---|
| 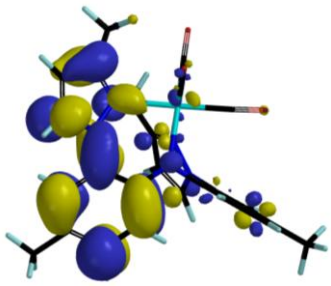 | 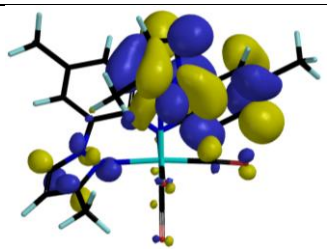 | 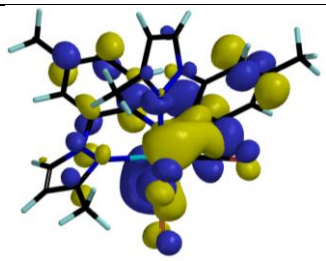 |
| **-1.01** | **-0.62 eV** | **-0.28 eV** |
| **α-LUMO** | **α-LUMO(+1)** | **α-LUMO(+2)** |

| | | |
|---|---|---|
| 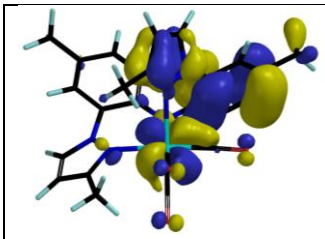 | 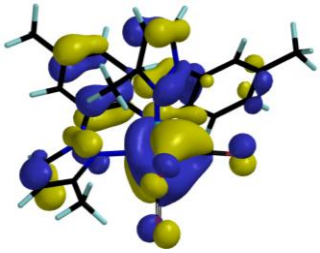 | 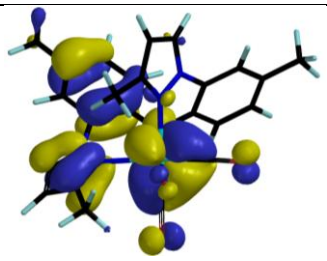 |
| **-11.60 eV** | **-11.81 eV** | **-11.90 eV** |
| **α-HOMO** | **α-HOMO(-1)** | **α-HOMO(-2)** |

| | | |
|---|---|---|
| 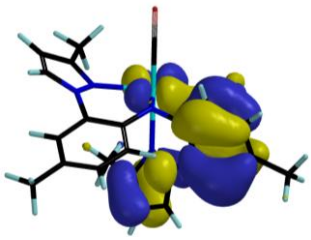 | 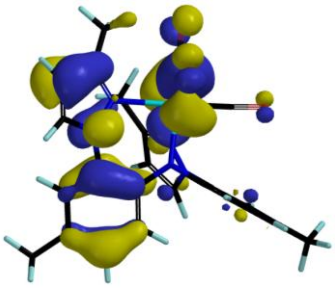 | 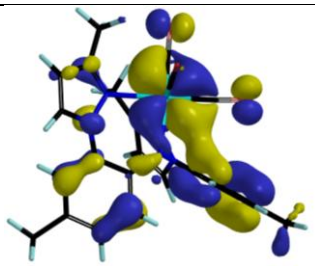 |
| **-12.26 eV** | **-12.48 eV** | **-12.82 eV** |
| **α-HOMO(-3)** | **α-HOMO(-4)** | **α-HOMO(-5)** |

**Fig. S-30.** Beta-Frontier Orbitals for [*fac*-Re(CO)$_3$(**L**$^{\mathbf{Me}}$)$^+$], (**3**$^{\mathbf{Me+}}$) from DFT calculations (uB3LYP/LACVP*).

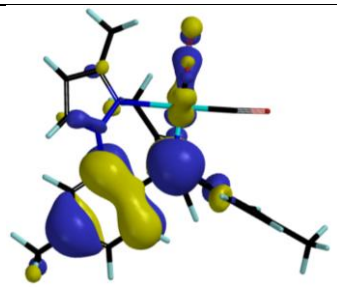

**-0.149 eV**

**β-LUMO**

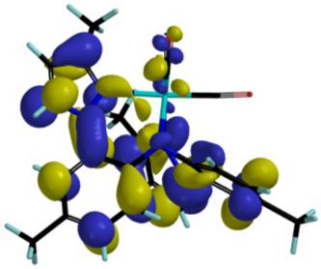

**-0.029 eV**

**β-LUMO(+1)**

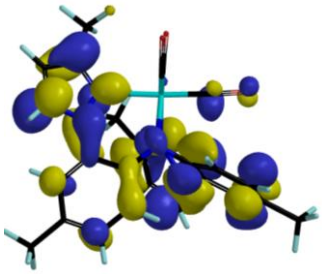

**-0.019 eV**

**β-LUMO(+2)**

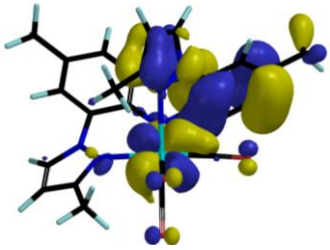

**-0.426 eV**

**β-HOMO**

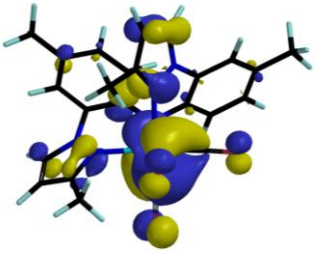

**-0.428 eV**

**β-HOMO(-1)**

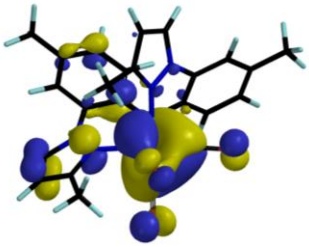

**-0.439 eV**

**β-HOMO(-2)**

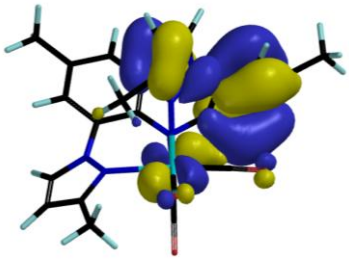

**-0.450 eV**

**β-HOMO(-3)**

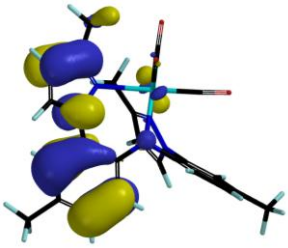

**-0.457 eV**

**β-HOMO(-4)**

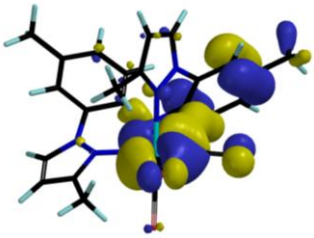

**-0.470 eV**

**β-HOMO(-5)**

**Figure S-31**. Overlay of Calculated Absorption Spectra of **3**$^{H}$, **3**$^{Me}$, **3**$^{iPr}$, and (**3**$^{Me+}$).

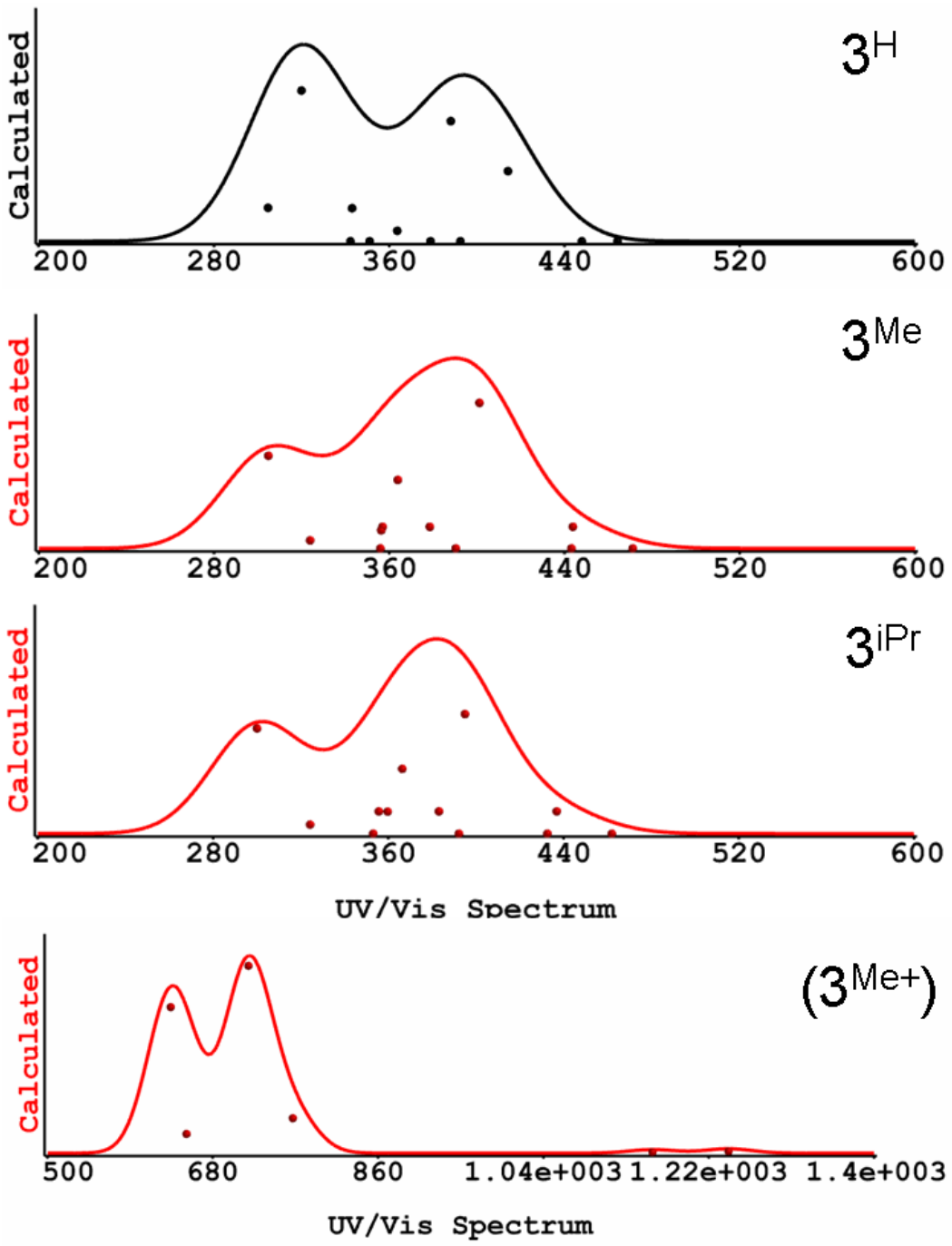

**Table S-1.** TDDFT/TDA Excitation Energies For Transitions of *fac*-Re(CO)$_3$(**L$^{Me}$**), **3$^{Me}$.**

| Excited State | Total Energy (hartrees) | Excitation energy (eV) | Strength | Origin | Amplitude | Transition moment X | Y | Z |
|---|---|---|---|---|---|---|---|---|
| | | | | Singlet Transitions | | | | |
| **1** | -1544.467129551245 | 2.7935 | 0.0077 | D(123)→V(1) | 0.9903 | -0.2866 | -0.1752 | -0.0189 |
| **2** | -1544.456209333911 | 3.0907 | 0.0522 | D(123)→V(2) | 0.9802 | -0.7140 | 0.4107 | -0.1023 |
| **3** | -1544.444581304328 | 3.4071 | 0.0246 | D(123)→V3) | 0.8724 | 0.4540 | 0.2940 | -0.0438 |
| | | | | D(123)→V(4) | -0.4429 | | | |
| **4** | -1544.441930439744 | 3.4792 | 0.0065 | D(123)→V3) | 0.4270 | 0.1948 | -0.0075 | -0.1955 |
| | | | | D(123)→V(4) | 0.8658 | | | |
| **5** | -1544.429107806090 | 3.8282 | 0.0029 | D(123)→V(5) | 0.9732 | 0.1680 | 0.0283 | -0.0400 |
| **6** | -1544.420318817385 | 4.0673 | 0.0332 | D(121)→V(1) | 0.6823 | -0.4481 | 0.0523 | 0.3600 |
| | | | | D(122)→V(2) | 0.6190 | | | |
| | | | | Triplet Transitions | | | | |
| **1** | -1544.473078819383 | 2.6316 | 0.0000 | D(123)→V(1) | 0.6685 | 0.0000 | 0.0000 | 0.0000 |
| | | | | D(123)→V(2) | 0.7015 | | | |
| **2** | -1544.466979581862 | 2.7976 | 0.0000 | D(123)→V(1) | 0.7329 | 0.0000 | 0.0000 | 0.0000 |
| | | | | D(123)→V(2) | -0.6609 | | | |
| **3** | -1544.453076563946 | 3.1759 | 0.0000 | D(123)→V(3) | 0.8427 | 0.0000 | 0.0000 | 0.0000 |
| | | | | D(123)→V(4) | 0.4197 | | | |
| **4** | -1544.449413883842 | 3.2756 | 0.0077 | D(123)→V(3) | -0.4041 | 0.0000 | 0.0522 | 0.0000 |
| | | | | D(123)→V(4) | 0.8513 | | | |
| **5** | -1544.442139133860 | 3.4736 | 0.0077 | D(118)→V(1) | -0.3538 | 0.0246 | 0.0077 | 0.0000 |
| | | | | D(121)→V(1) | 0.3895 | | | |
| | | | | D(122)→V(1) | 0.6363 | | | |
| **6** | -1544.441786879920 | 3.4831 | 0.0000 | D(123)→V(6) | -0.4694 | 0.0000 | 0.0000 | 0.0000 |
| | | | | D(123)→V(7) | -0.5068 | | | |
| | | | | D(123)→V(8) | 0.4754 | | | |

Key: D(123) = HOMO, D(122) = HOMO(-1); V(1) = LUMO, V(2) = LUMO(+1), etc.

**Table S-2.** TDDFT/TDA Excitation Energies For Transitions of *fac*-Re(CO)$_3$(**L**$^{iPr}$), **3**$^{iPr}$.

| Excited State | Total Energy (hartrees) | Excitation energy (eV) | Strength | Origin | Amplitude | Transition moment X | Y | Z |
|---|---|---|---|---|---|---|---|---|
| | | | | Singlet Transitions | | | | |
| **1** | -1701.715589591982 | 2.8381 | 0.0085 | D(139)→V(1) | 0.9901 | -0.3185 | -0.1420 | 0.0141 |
| **2** | -1701.704544497414 | 3.1387 | 0.0455 | D(139)→V(2) | 0.9812 | -0.6297 | 0.4398 | -0.0432 |
| **3** | -1701.695514001197 | 3.3844 | 0.0247 | D(139)→V3) | 0.8410 | 0.4748 | 0.2680 | -0.0134 |
| | | | | D(139→V(4) | -0.4958 | | | |
| **4** | -1701.693214969075 | 3.4470 | 0.0084 | D(139)→V3) | 0.4830 | 0.2353 | -0.170 | -0.2095 |
| | | | | D(139→V(4) | 0.8382 | | | |
| **5** | -1701.679398048736 | 3.8230 | 0.0035 | D(139)→V(5) | 0.9717 | 0.1722 | 0.0675 | -0.0514 |
| **6** | -1701.668066786418 | 4.1313 | 0.0400 | D(138)→V(1) | 0.8718 | -0.2666 | -0.0077 | 0.5694 |
| | | | | D(138)→V(2) | 0.2279 | | | |
| | | | | Triplet Transitions | | | | |
| **1** | -1701.721274104852 | 2.6834 | 0.0000 | D(139)→V(1) | 0.7553 | 0.0000 | 0.0000 | 0.0000 |
| | | | | D(139)→V(2) | 0.6003 | | | |
| **2** | -1701.714563531595 | 2.8661 | 0.0000 | D(139)→V(1) | -0.6414 | 0.0000 | 0.0000 | 0.0000 |
| | | | | D(139)→V(2) | 0.7372 | | | |
| **3** | -1701.703722770954 | 3.1610 | 0.0000 | D(139)→V(3) | 0.8092 | 0.0000 | 0.0000 | 0.0000 |
| | | | | D(139)→V(4) | 0.4687 | | | |
| **4** | -1701.700955263776 | 3.2364 | 0.0085 | D(139)→V(3) | -0.4451 | 0.0000 | 0.0455 | 0.0000 |
| | | | | D(139)→V(4) | 0.8260 | | | |
| **5** | -1701.691765459548 | 3.4864 | 0.0085 | D(139)→V(6) | -0.6623 | 0.0247 | 0.0000 | 0.0000 |
| | | | | D(139)→V(7) | 0.2569 | | | |
| | | | | D(139)→V(9) | 0.5309 | | | |
| **6** | -1701.691765459548 | 3.4864 | 0.0085 | D(134)→V(1) | -0.3639 | 0.0000 | 0.0000 | 0.0000 |
| | | | | D(137)→V(1) | 0.2427 | | | |
| | | | | D(138)→V(1) | 0.7147 | | | |

Key: D(139) = HOMO, D(138) = HOMO(-1); V(1) = LUMO, V(2) = LUMO(+1), etc.

**Table S-3.** TDDFT/TDA Excitation Energies For Transitions of [*fac*-Re(CO)$_3$(**L$^{Me}$**)$^+$], (**3$^{Me+}$**).

| Excited State | Total Energy (hartrees) | Excitation energy (eV) | Strength | Origin | Amplitude | Transition moment X | Y | Z |
|---|---|---|---|---|---|---|---|---|
| **1** | -1544.320297098923 | 0.9986 | 0.0017 | D(122)→S(1) | 0.9923 β | -0.2479 | -0.0843 | 0.0107 |
| | <S**2> = 0.7754 | | | | | | | |
| **2** | -1544.317674736288 | 1.0699 | 0.0014 | D(120)→S(1) | 0.1791 β | -0.1272 | 0.1865 | -0.0249 |
| | <S**2> = 0.7760 | | | D(121)→S(1) | 0.9784 β | | | |
| **3** | -1544.297606159928 | 1.6160 | 0.0144 | D(117)→S(1) | 0.1666 β | 0.0101 | 0.6026 | 0.00041 |
| | <S**2> = 0.7757 | | | D(118)→S(1) | 0.2963 β | | | |
| | | | | D(119)→S(1) | 0.7552 β | | | |
| | | | | D(120)→S(1) | -0.5347 β | | | |
| **4** | -1544.293620000055 | 1.7245 | 0.0728 | D(117)→S(1) | 0.1946 β | -0.1366 | -1.3038 | 0.0746 |
| | <S**2> = 0.7784 | | | D(118)→S(1) | -0.1780 β | | | |
| | | | | D(119)→S(1) | 0.5777 β | | | |
| | | | | D(120)→S(1) | 0.7451 β | | | |
| **5** | -1544.287059299183 | 1.9030 | 0.0084 | D(117)→S(1) | 0.6720 β | -0.0306 | -0.4231 | 0.0007 |
| | <S**2> = 0.7756 | | | D(118)→S(1) | 0.6534 β | | | |
| | | | | D(119)→S(1) | -0.2733 β | | | |
| | | | | D(120)→S(1) | 0.1780 β | | | |
| **6** | -1544.285165188011 | 1.9546 | 0.0570 | D(117)→S(1) | 0.6755 β | -0.6545 | 0.8727 | -0.0224 |
| | <S**2> = 0.0017 | | | D(118)→S(1) | -0.6504 β | | | |
| | | | | D(120)→S(1) | -0. 2518 β | | | |

Key: D(122) = β-HOMO, D(121) = β-HOMO(-1) , etc.; S(1) = SOMO

**Table S-4.** Cartesian Coordinates of *fac*-Re(CO)$_3$(**L$^{Me}$**), **3$^{Me}$**

Standard Nuclear Orientation (Angstroms)

| I | Atom | X | Y | Z |
|---|---|---|---|---|
| 1 | Re | -0.649297 | 0.671355 | -1.855180 |
| 2 | O | 0.869243 | 0.405620 | -4.526427 |
| 3 | O | -2.505133 | 2.911785 | -2.901071 |
| 4 | O | -2.757568 | -1.271735 | -2.992834 |
| 5 | N | -1.594415 | 0.664718 | 0.199121 |
| 6 | N | -1.824341 | -0.527994 | 0.833760 |
| 7 | N | 1.037285 | 2.059096 | -1.218359 |
| 8 | N | 2.126889 | 1.571278 | -0.538447 |
| 9 | N | 0.475731 | -0.869596 | -0.744947 |
| 10 | C | -1.965869 | 1.629191 | 1.055304 |
| 11 | C | -2.438166 | 1.054289 | 2.250955 |
| 12 | H | -2.776270 | 1.579061 | 3.132739 |
| 13 | C | -2.329981 | -0.308585 | 2.072654 |
| 14 | H | -2.572589 | -1.135972 | 2.723008 |
| 15 | C | -1.572846 | -1.795699 | 0.224385 |
| 16 | C | -2.492912 | -2.828527 | 0.394196 |
| 17 | H | -3.420290 | -2.647703 | 0.933136 |
| 18 | C | -2.265198 | -4.084815 | -0.183650 |
| 19 | C | -1.110204 | -4.253746 | -0.958962 |
| 20 | H | -0.917652 | -5.212365 | -1.436135 |
| 21 | C | -0.197878 | -3.213071 | -1.141497 |
| 22 | H | 0.702820 | -3.358963 | -1.731541 |
| 23 | C | -0.403144 | -1.965137 | -0.553224 |
| 24 | C | -3.253706 | -5.211985 | 0.017933 |
| 25 | H | -3.043044 | -6.036947 | -0.670203 |
| 26 | H | -4.285249 | -4.879690 | -0.149312 |
| 27 | H | -3.184121 | -5.610170 | 1.039441 |
| 28 | C | 1.479691 | 3.145788 | -1.889438 |
| 29 | C | 2.843453 | 3.352916 | -1.634241 |
| 30 | H | 3.461047 | 4.135931 | -2.050270 |
| 31 | C | 3.225131 | 2.320905 | -0.804244 |
| 32 | H | 4.188465 | 2.049079 | -0.400980 |
| 33 | C | 2.072613 | 0.562225 | 0.471132 |
| 34 | C | 2.853703 | 0.802578 | 1.610610 |
| 35 | H | 3.353108 | 1.763588 | 1.702531 |
| 36 | C | 3.011577 | -0.136876 | 2.620307 |
| 37 | C | 2.338694 | -1.357448 | 2.447979 |
| 38 | H | 2.457938 | -2.131956 | 3.204811 |
| 39 | C | 1.522802 | -1.594357 | 1.354254 |
| 40 | H | 1.020128 | -2.552910 | 1.298007 |
| 41 | C | 1.321212 | -0.637163 | 0.316544 |
| 42 | C | 3.851396 | 0.141828 | 3.844459 |
| 43 | H | 4.331804 | 1.124368 | 3.772094 |

44 H 4.650642 -0.600441 3.970934
45 H 3.251836 0.154690 4.764951
46 C 0.291241 0.508280 -3.523501
47 C -1.963834 -0.555996 -2.536752
48 C -1.772871 2.076345 -2.543341
49 C -1.848733 3.084884 0.725469
50 H -0.794809 3.347804 0.581326
51 H -2.269849 3.693790 1.531070
52 H -2.404543 3.359873 -0.176547
53 C 0.633979 3.975127 -2.796721
54 H -0.316562 4.272472 -2.346909
55 H 0.395717 3.462367 -3.735356
56 H 1.162927 4.898612 -3.053017
---

**Table S-5.** Cartesian Coordinates of *fac*-Re(CO)$_3$(**L**$^{iPr}$), **3**$^{iPr}$

Cartesian Coordinates (Angstroms)

| Atom | X | Y | Z |
|---|---|---|---|
| 1 Re | Re1 | -0.2979520 | 1.0881576 | 0.3843912 |
| 2 O | O1 | -1.3027005 | 2.0450952 | 3.1507862 |
| 3 O | O3 | -1.9263802 | 3.1979571 | -1.2052865 |
| 4 O | O2 | 1.7881687 | 3.3614394 | 0.5611797 |
| 5 N | N1 | 0.5853435 | 0.2288048 | -1.4933766 |
| 6 N | N2 | 1.9440255 | -0.0184515 | -1.5489332 |
| 7 N | N3 | -1.9045598 | -0.5329418 | 0.5286228 |
| 8 N | N4 | -1.5588447 | -1.7362764 | 1.1297958 |
| 9 N | N5 | 1.0904210 | -0.4662363 | 1.1021565 |
| 10 C | C1 | 0.0778938 | -0.1688133 | -2.6846842 |
| 11 C | C2 | 1.1188945 | -0.6673945 | -3.5096484 |
| 12 H | H2A | 1.0267682 | -1.0727468 | -4.5156449 |
| 13 C | C3 | 2.2776352 | -0.5624488 | -2.7579791 |
| 14 H | H3A | 3.3046579 | -0.8594103 | -2.9609572 |
| 15 C | C4 | 2.8367011 | 0.2618294 | -0.4676346 |
| 16 C | C5 | 4.1086983 | 0.7831871 | -0.7452232 |
| 17 H | H5A | 4.3770878 | 1.0286932 | -1.7797204 |
| 18 C | C6 | 5.0237227 | 1.0310043 | 0.2961512 |
| 19 C | C7 | 4.6089858 | 0.7705280 | 1.6167482 |
| 20 H | H7A | 5.2966311 | 0.9777742 | 2.4453967 |
| 21 C | C8 | 3.3286368 | 0.2677690 | 1.8951915 |
| 22 H | H8A | 3.0104486 | 0.0771205 | 2.9254761 |
| 23 C | C9 | 2.4129671 | 0.0013637 | 0.8628752 |
| 24 C | C10 | 6.4091960 | 1.5618934 | -0.0067992 |
| 25 H | H10A | 6.8462179 | 2.0697074 | 0.8697377 |
| 26 H | H10B | 6.3937460 | 2.2821988 | -0.8436025 |
| 27 H | H10C | 7.1003138 | 0.7450206 | -0.2918152 |
| 28 C | C11 | -3.2368072 | -0.3640471 | 0.7864000 |
| 29 C | C12 | -3.7243408 | -1.4440463 | 1.5559953 |
| 30 H | H12A | -4.7373131 | -1.5807721 | 1.9304116 |
| 31 C | C13 | -2.6391678 | -2.2798640 | 1.7626521 |
| 32 H | H13A | -2.5385959 | -3.2146886 | 2.3097490 |
| 33 C | C14 | -0.3510049 | -2.4546736 | 0.8683683 |
| 34 C | C15 | -0.4911105 | -3.8354613 | 0.6143826 |
| 35 H | H15A | -1.5044901 | -4.2423977 | 0.5186651 |
| 36 C | C16 | 0.6079839 | -4.6886753 | 0.4608659 |
| 37 C | C17 | 1.8828864 | -4.0907794 | 0.5574429 |
| 38 H | H17A | 2.7813414 | -4.7131384 | 0.4528261 |
| 39 C | C18 | 2.0384131 | -2.7219901 | 0.7617982 |
| 40 H | H18A | 3.0488998 | -2.3087739 | 0.8223186 |
| 41 C | C19 | 0.9305235 | -1.8259665 | 0.9142566 |
| 42 C | C20 | 0.4369376 | -6.1702976 | 0.2036725 |
| 43 H | H20A | -0.6211406 | -6.4278918 | 0.0214929 |

44 H H20B 0.7808229 -6.7793479 1.0623444
45 H H20C 1.0176987 -6.5030386 -0.6769078
46 C C21 -0.9362962 1.6836457 2.0927436
47 C C22 1.0257969 2.4698768 0.4777006
48 C C23 -1.3563021 2.3865785 -0.5622591
49 C C24 -1.3951515 -0.0876125 -3.0039150
50 H H24A -1.8983346 0.2951355 -2.0983701
51 C C25 -4.0625865 0.8046847 0.3011218
52 H H25A -3.4077614 1.4651173 -0.2858879
53 C C26 -1.6638104 0.8961172 -4.1640815
54 H H2 -1.3187099 1.9131336 -3.9126596
55 H H3 -2.7463311 0.9454526 -4.3782930
56 H H4 -1.1500220 0.5751818 -5.0887638
57 C C27 -1.9641244 -1.4925968 -3.3040344
58 H H1 -1.5116908 -1.9245828 -4.2156720
59 H H5 -3.0554675 -1.4360674 -3.4676093
60 H H6 -1.7739409 -2.1862838 -2.4672242
61 C C28 -4.6348064 1.6262070 1.4785052
62 H H7 -3.8330968 2.0011456 2.1354188
63 H H8 -5.3223041 1.0175212 2.0944275
64 H H9 -5.2032786 2.4921499 1.0947224
65 C C29 -5.1923069 0.3125344 -0.6332214
66 H H10 -5.8910233 -0.3615051 -0.1049419
67 H H11 -4.7868018 -0.2357557 -1.5014896
68 H H12 -5.7736758 1.1736878 -1.0084093

**Table S-6.** Cartesian Coordinates of [*fac*-Re(CO)$_3$(**L$^{Me}$**)$^+$], (**3$^{Me+}$**)

Standard Nuclear Orientation (Angstroms)

| I | Atom | X | Y | Z |
|---|---|---|---|---|
| 1 | Re | -0.454210 | 1.232300 | 0.167758 |
| 2 | O | -1.530734 | 2.340681 | 2.836976 |
| 3 | O | -1.675036 | 3.524962 | -1.508792 |
| 4 | O | 1.977055 | 3.100394 | 0.505146 |
| 5 | N | 0.444565 | 0.211305 | -1.638680 |
| 6 | N | 1.702162 | -0.326906 | -1.555174 |
| 7 | N | -2.315550 | -0.075670 | 0.144237 |
| 8 | N | -2.286911 | -1.344361 | 0.670626 |
| 9 | N | 0.541606 | -0.555986 | 0.994329 |
| 10 | C | -0.012270 | -0.077667 | -2.867106 |
| 11 | C | 0.957502 | -0.808053 | -3.580717 |
| 12 | H | 0.862897 | -1.205560 | -4.580857 |
| 13 | C | 2.023434 | -0.947177 | -2.717379 |
| 14 | H | 2.980599 | -1.433119 | -2.836058 |
| 15 | C | 2.526649 | -0.203666 | -0.394702 |
| 16 | C | 3.885358 | 0.065096 | -0.548873 |
| 17 | H | 4.296100 | 0.239988 | -1.540784 |
| 18 | C | 4.718371 | 0.180112 | 0.572234 |
| 19 | C | 4.137068 | 0.051928 | 1.840821 |
| 20 | H | 4.755918 | 0.156395 | 2.729545 |
| 21 | C | 2.772770 | -0.201007 | 1.993713 |
| 22 | H | 2.334541 | -0.314487 | 2.981524 |
| 23 | C | 1.938151 | -0.339116 | 0.884715 |
| 24 | C | 6.197053 | 0.451273 | 0.404113 |
| 25 | H | 6.649124 | 0.729396 | 1.361584 |
| 26 | H | 6.380556 | 1.262001 | -0.311092 |
| 27 | H | 6.717039 | -0.446832 | 0.043708 |
| 28 | C | -3.594059 | 0.344798 | 0.269094 |
| 29 | C | -4.377842 | -0.653110 | 0.867207 |
| 30 | H | -5.429855 | -0.584860 | 1.104324 |
| 31 | C | -3.512165 | -1.691194 | 1.136657 |
| 32 | H | -3.663952 | -2.634338 | 1.638617 |
| 33 | C | -1.191110 | -2.252542 | 0.548925 |
| 34 | C | -1.533259 | -3.577088 | 0.241040 |
| 35 | H | -2.571498 | -3.803834 | 0.012914 |
| 36 | C | -0.599461 | -4.603940 | 0.216926 |
| 37 | C | 0.726182 | -4.249223 | 0.515441 |
| 38 | H | 1.485342 | -5.030392 | 0.533534 |
| 39 | C | 1.091976 | -2.938470 | 0.772660 |
| 40 | H | 2.137261 | -2.737072 | 0.976348 |
| 41 | C | 0.158429 | -1.860431 | 0.777018 |
| 42 | C | -0.984750 | -6.024148 | -0.123779 |
| 43 | H | -2.066767 | -6.108296 | -0.277315 |

44 H -0.716319 -6.725197 0.677613
45 H -0.509988 -6.371788 -1.051513
46 C -1.125185 1.929781 1.828424
47 C 1.080999 2.373047 0.369663
48 C -1.246154 2.670587 -0.839284
49 C -1.373759 0.333322 -3.335067
50 H -2.138894 -0.156620 -2.722545
51 H -1.515546 0.058715 -4.384631
52 H -1.527937 1.415986 -3.287700
53 C -4.078884 1.694478 -0.142614
54 H -3.774589 1.970857 -1.155180
55 H -3.726696 2.489560 0.524120
56 H -5.173255 1.714484 -0.126817

## *[F] References*


[S1] S. Wanniarachchi; B.J. Liddle; J. Toussaint; S.V. Lindeman; B. Bennett; J.R. Gardinier *Dalton Trans.* 39 (2010) 3167 – 3169.

[S2] SPARTAN, Wavefunction, Inc., Irvine, CA, 1997.

[S3] For instance see: (a) T. Takatani, J. S. Sears, D. C. Sherill, J. Phys. Chem. A 113 (2009) 9231-9236. (b) V.M. Rayon, G. Frenking, Chem. Eur. J. 8 (2002) 4693-4707. (c) R.K. Szilagyi, G. Frenking, Organometallics 16 (1997) 4807-4815.

[S4] A. D. Becke, J. Chem. Phys. 98 (1993) 5648-5652.

[S5] C. Lee, W. Yang, R.G. Parr, Phys. Rev. B 37 (1988) 785-789.

[S6] (a) P. J. Hay, W.R. Wadt, J. Chem. Phys. 82 (1985) 270-283. (b) W.R. Wadt, P.J. Hay, J. Chem. Phys. 82 (1985) 284-298.